D5.3 MHVM for CH and non-CH elements

Deliverable number	**D5.3**
Deliverable title	**MHVM for CH and non-CH elements**
Nature[1]	**R**
Dissemination Level [2]	**PU**
Author (email) Institution	**emontes@ugr.es** **UGR**
Editor (email) Institution	
Leading partner	**UGR**
Participating partners	**UGR, OSMU, NTUA, UNIPD, IUAV, RED**
Official submission date:	**31/08/2020**
Actual submission date:	**27/08/2020**

[1] **R**=Document, report; **DEM**=Demonstrator, pilot, prototype; **DEC**=website, patent fillings, videos, etc.; **OTHER**=other

[2] **PU**=Public, **CO**=Confidential, only for members of the consortium (including the Commission Services), **CI**=Classified, as referred to in Commission Decision 2001/844/EC

Modifications Index	
Date	Version
21/06/2020	0.1 First draft
24/06/2020	0.2 Second draft
29/06/2020	0.3 Updated structure and inclusion of MHVM xml format
27/07/2020	0.4 Updated structure and inclusion of materials deterioration, and the applicable assets
01/08/2020	0.5 Review by NTUA
04/08/2020	1.0 First version

This work is a part of the HYPERION project. HYPERION has received funding from the European Union's Horizon 2020 research and innovation programme under grant agreement no 821054.

ACRONYMS AND ABBREVIATIONS

$AvgS_a$	Average Spectral Acceleration
C	Capacity
CC	Climate Change
CH	Cultural Heritage
D	Demand
DM	Damage Measure
EDP	Engineering Demand Parameter
HRAP	Holistic Risk Assessment Platform
IM	Intensity Measure
LS	Limit State
MHVM	Multi-Hazard Vulnerability Module
MSA	Multi-Stripe Analysis
PGA	Peak Ground Acceleration
R_{eq}	Equivalent ice thickness accumulated on a member
u_{10}	10-minute mean wind speed measured at 10m height from the ground

Table of Contents

Table of Figures

Table of Tables

Executive Summary

Deliverable D5.3 “MHVM for CH and non-CH elements” documents the work performed in Task 5.3 “Development of vulnerability modules” during the first fifteen months of the project’s duration.

This deliverable includes the structure, purpose and use of Multi-Hazard Vulnerability Modules (MHVMs) for cultural heritage (CH) and non-CH assets within the HYPERION platform. In particular, MHVMs are software and data libraries with a standardizable format that encode the results of structural vulnerability assessment and enable a seamless integration of hazard simulators, structural analysis and consequence models into the HRAP model of CH and non-CH assets for each case-study city (Granada, Rhodes, Tønsberg, Venice). The assets are classified in Tier 1, Tier 2 and Tier 3 categories, depending on the modelling and monitoring resolution. For Tier 1, structure-specific models are developed and asset-specific fragility and consequence functions are used, while sensors are also employed to connect the model with reality. For the inventory in Tier 2, only important CH and non-CH assets are considered, typically to the same level of detail as Tier 1, but without any sensor input. For Tier 3, a generic model is provided and only a limited number of characteristic “index” assets that better represent the entire class are selected and generic fragility and consequence functions are employed for risk assessment. All potential hazards of importance to each asset are taken into account. The entire range of physical and weather stressors is applied to the structural models to assess the assets’ response and the associated damage. The results are encoded into the MHVM that describes each structure (Tier 1,2) or category of structures (Tier 3). In this way, the rehabilitation/emergency action planning is firmly supported by the assessment of vulnerability, loss and downtime.

1 Introduction

1.1 Background

The deliverable D5.3 “MHVM for CH and non-CH elements” is an important document, establishing the framework that enables the information flow from hazard to component state and system risk/resilience.

All the information gathered within the D5.3 document will be encoded in software libraries that will enable a seamless integration of hazard simulators and vulnerability results into the HRPAP of the system.

1.2 Scope and Objective

The objective is to obtain the vulnerability results of CH (buildings, bridges, monuments, etc.) and non-CH assets (slopes, electrical substations, antennas, non-CH buildings/bridges, etc.) due to multi-hazards, such us climate-related loads (snow, rain, wind, etc.), geo-hazard intensities (e.g., ground acceleration) or man-made hazards (e.g., fire loads).

The deliverable is offered in two versions. The first version, to be delivered by M15, focuses on the initial development of the MHVM structure and corresponding software, containing examples of non-CH assets only. The second version (by M24) will refine the MHVM structure according to implementation findings and also include examples of application on CH assets.

1.3 Definitions

Hazard: stressors associated with a peril that may affect the normal activities of people and the integrity and functionality of CH and non-CH assets, including, for example, ground shaking for earthquakes or wind action for storms.

Intensity Measure: an interface variable that is employed between the hazard analysis and the structural analysis.

Engineering Demand Parameter: structural response quantity used to estimate damage to structural and non-structural components and systems.

Fragility curve: function that provides the probability of exceeding a given limit state, or equivalently of being in a damage state or worse, given the intensity measure.

Vulnerability curve: function that provides the distribution of a loss measure given the level of the intensity measure.

Exposure model: it contains information on the assets at risk, their location, taxonomy, etc.

Material degradation: deterioration of the mechanical properties of the material and/or loss of material mass with time when exposed to the environment.

Landslide: a collapse or substantial movement of a mass of earth or rock from a mountain or cliff.

Vandalism: action involving deliberate destruction of or damage to public or private property.

1.4 Position in the HYPERION Ecosystem

The HYPERION high-level logical architecture is presented in Figure 1, as defined in Deliverable D2.3 "Architecture Specification" (Krommyda et al. 2020). The dashed red rectangle shows the position of the Multi-Hazard Vulnerability Module (WP5) in the HYPERION Ecosystem. Essentially, MHVMs are created offline via the Structural and Geotechnical Safety Assessment simulator. In more detail, hazard simulators read hazard scenario inputs and feed their output into HRAP. HRAP in turns feeds the hazard input into MHVMs for performing risk and resilience assessment, the results of which are returned back to the middleware for storage.

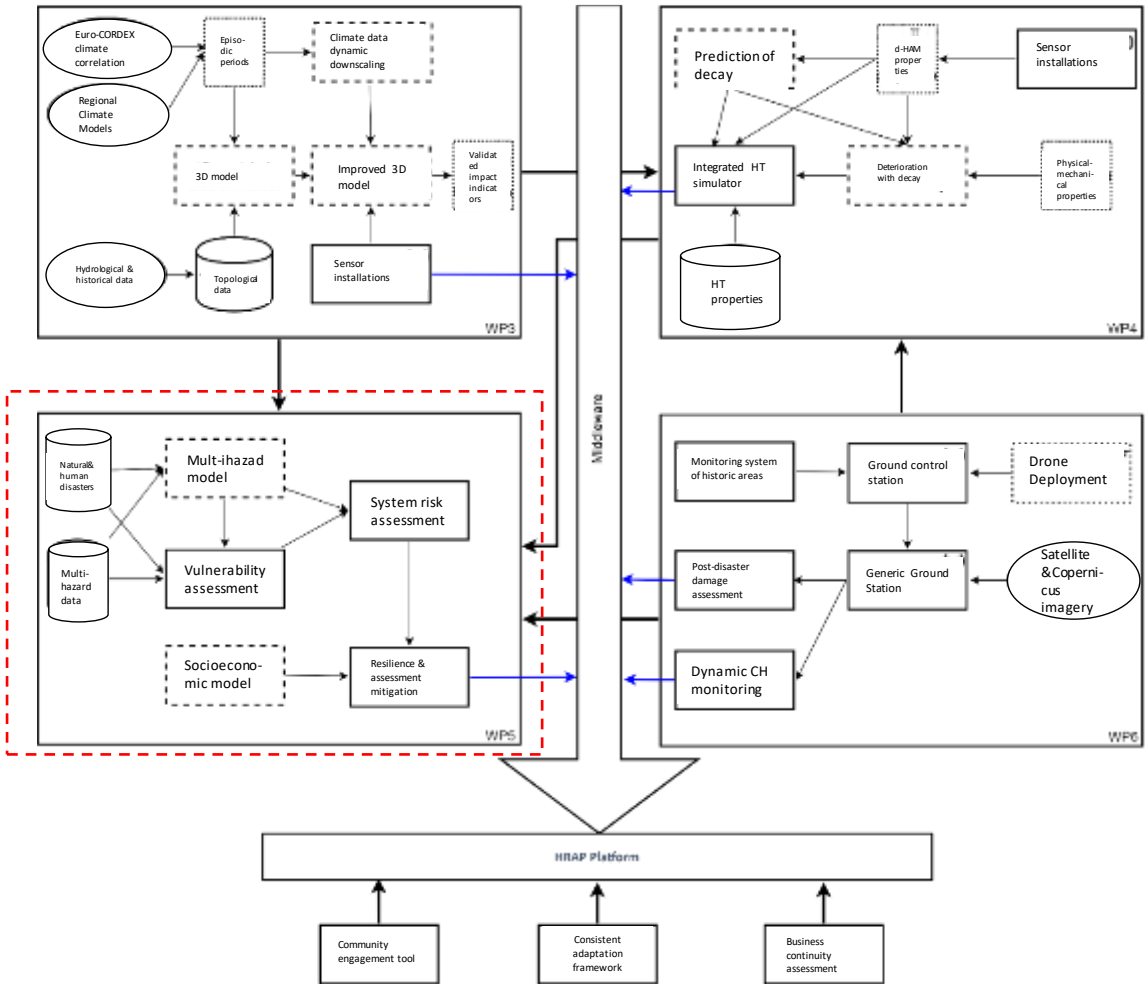

(a) Entire HYPERION Ecosystem

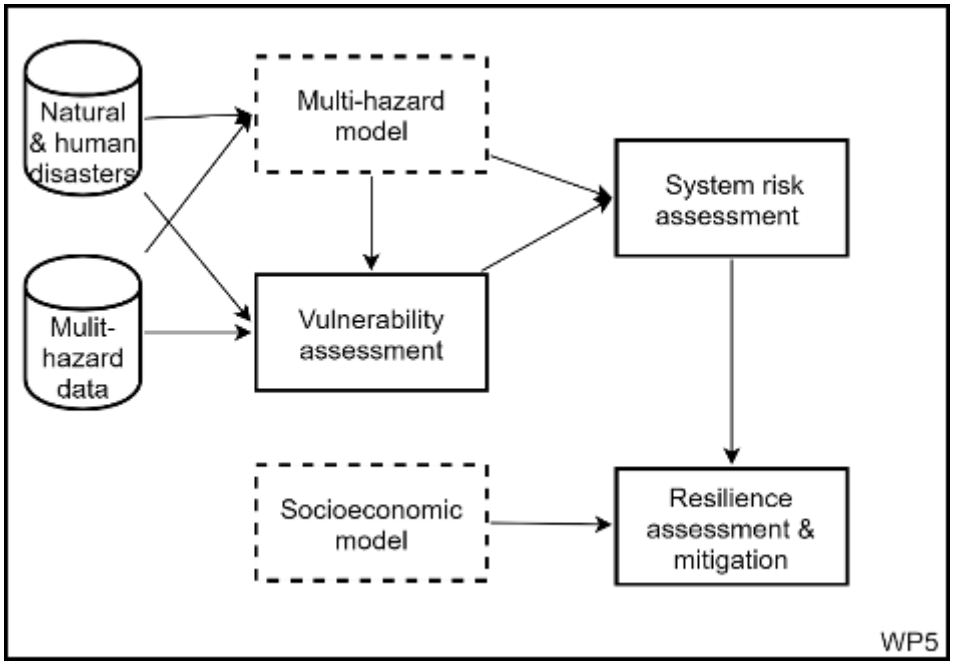

(b) WP5 module: MHVM

Figure 1: Position of the MHVM within the HYPERION Ecosystem, at the heart of "Vulnerability assessment".

2 Theoretical implications

2.1 IM approach

The analytical estimation of losses involves the combination of hazard (climate-related, geo-hazard and man-made hazard) with the results of (geo)structural analyses evaluated by engineers. Typically, an interface variable is employed between the hazard analysis and (geo)structural analysis, which is called the Intensity Measure (IM). IM stands for a point of contact between the different disciplines attempting to incorporate all complexity of the hazard-specific loading into a single quantity that can be used for the (geo)structural analysis. The aim is to avoid considering all the diverse characteristics of the loading. Considering earthquakes, for example, seismologists estimate the statistical properties of the IM through Probabilistic Seismic Hazard Analysis (Cornell 1968), while engineers assess the structural response for a given level of IM without considering a complex combination of earthquake magnitude, source – structure distance and other relevant seismological parameters. The desirable decoupling is achieved by selecting an appropriate IM that is efficient and sufficient with respect to the characteristics of the hazard examined (Luco and Cornell 2007).

IM efficiency means that the selected IM should be a good predictor of the (geo)structural response, as measured by the asset's Engineering Demand Parameter (EDP) of interest. This enables achieving the desirable level of confidence on the numerical analysis results with a small number of time-history analyses. IM sufficiency means that the IM should render an asset's response independent of other characteristics of the hazard. A sufficient IM selected for seismic risk assessment would remove any bias from considering the magnitude, distance and other seismological parameters of the ground motion records rather than the IM. The goals of efficiency and sufficiency are not necessarily the same, as the former aims at reducing the variability in the dynamic analysis results, while the latter at reducing the dependence of the results on other characteristics of the hazard rather than the IM. Note that the reduction in the response dispersion gained by an efficient IM does not necessarily mean that the overall risk variability is reduced, since part of the variability is simply shifted to a different level within the risk estimation assessment.

In the HYPERION framework, for each type of hazard an appropriate IM is selected, as presented in Table 1. In the case of geo-hazard (earthquake), *PGA* is the peak ground acceleration, $Sa(T_1)$ is the spectral acceleration at the fundamental period of the structure and *AvgSa* is the average spectral acceleration computed as the geomean of spectral acceleration values at different periods.

Table 1: Hazards considered in HYPERION and pertinent intensity measure (IM)

Hazard	**IM**
Weather	Wind speed/direction/gust factor, temperature, rainfall height, precipitation, ice thickness, etc.
Geo-hazard	*AvgSa*, *PGA*, $S_a(T_1)$

2.2 IM – EDP relationship approach

In the structural analysis context, each dynamic analysis provides a single pair of IM and demand EDP values. In view of uncertainties involved, multiple analyses on a considerable number of inputs are required for every level of the intensity considered. For instance, when examining the seismic hazard, multiple ground motion records are used as the input for the analysis at each level of the IM. There are many ways to group the aforementioned IM-EDP pairs in order to adequately characterize the IM-EDP space and estimate the demand, e.g. single-stripe analysis (Jalayer 2003), multi-stripe analysis (Jalayer 2003; Jalayer and Cornell 2009), cloud analysis (Jalayer 2003; Mackie and Stojadinovic 2001; Padgett and DesRoches 2008) or Incremental Dynamic Analysis (Vamvatsikos and Cornell 2002). In HYPERION, the multi-stripe analysis (MSA) method is selected for grouping the IM-EDP pairs as it allows easy post-processing without the need for fitting regression models.

In particular, multi-stripe analysis consists of a group of stripe analyses, each of which is performed at a different IM level. A single stripe consists of the structural analysis results when subjected to *n* time-histories of the hazard after being scaled at the certain IM level of the stripe. A characteristic exampled after Cornell and Jalayer (2002) is depicted in Figure 2, where each star indicates the non-linear time-history dynamic analysis result of the structure under a ground motion record that is scaled to $S_a(T_1)$ = 0.94g, where $S_a(T_1)$ is the spectral acceleration at the fundamental period of the structure. By conducting non-linear dynamic analyses for multiple intensity levels, the MSA results are obtained, as indicatively presented in Figure 3. It is noted that state-of-the-art tools are employed to selected the time-histories in order to deal with any IM insufficiency issues and better represent each IM level. In case of seismic hazard, for instance, the ground motion records are selected so as to be site-specific and hazard-consistent (Lin et al. 2013).

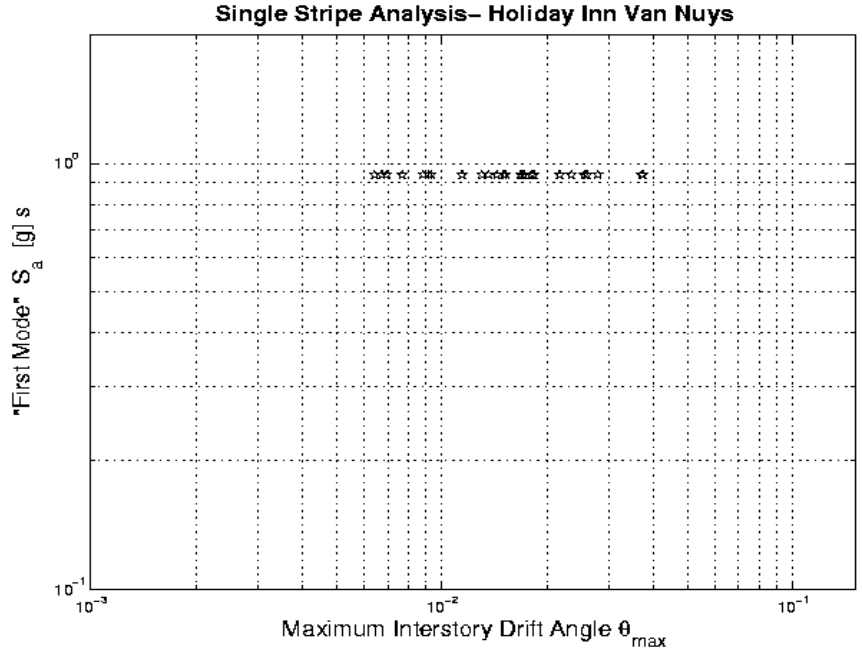

Figure 2: Single-stripe analysis results (Cornell and Jalayer 2002).

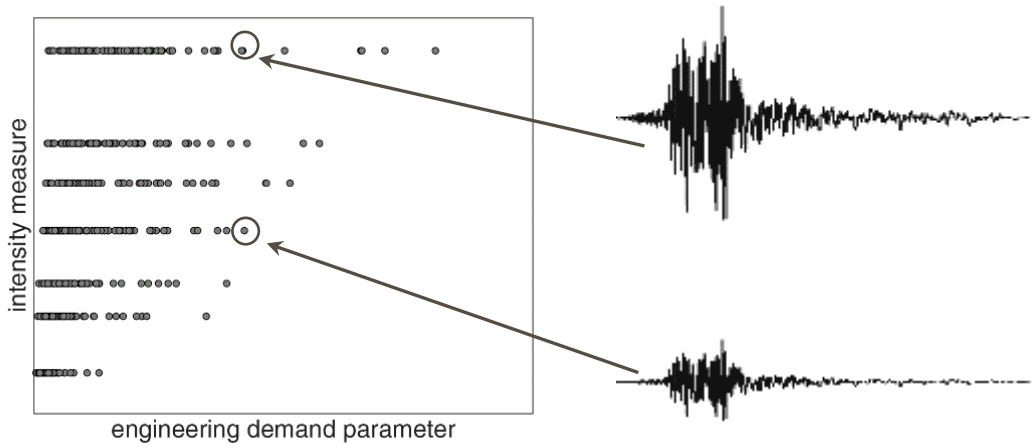

Figure 3: (a) Multi-stripe analysis results of an asset subjected to multiple ground motion time-histories and (b) scaled ground motion records used as the input for the analysis to get the IM-EDP pairs indicated by the two circles.

2.3 Performance assessment framework and the role of fragility and vulnerability

In HYPERION the Performance-Based Earthquake Engineering (PBEE) framework, originally developed by Cornell and Krawinkler (2000) for the Pacific Earthquake Engineering Research (PEER) Center, is employed for risk assessment. The PBEE methodology can be summarized as an implementation of the total probability theorem:

$$\lambda(DV) = \int_{DM}\int_{EDP}\int_{IM} G(DV \mid DM)\left|\mathrm{d}G(DM \mid EDP)\right|\left|\mathrm{d}G(EDP \mid IM)\right|\left|\mathrm{d}\lambda(IM)\right| \quad (1)$$

where *IM* is the intensity measure, *EDP* is the engineering demand parameter (e.g. maximum interstory drift ratio for a buildings), *DM* is the damage measure, *DV* is the decision variable and $G(var_1|var_2)$ is the probability that specified values of var_1 are exceeded given the level of var_2. The final product of this calculation is the mean annual frequency of exceeding *DV*, $\lambda(DV)$. Thus, risk can be estimated in terms of decision variables that make sense even to non-engineers, such as casualties, monetary loss, repair cost, or downtime. The approach for risk quantification is schematically shown in Figure 4.

- Exposure model: it contains information on the assets at risk, their location, taxonomy, value, vulnerability, etc. The CH and non-CH assets examined in HYPERION are classified to Tier 1, Tier 2 and Tier 3. Indicatively, the general urban plan of the city of Rhodes that shows the broad distribution of different classes of Tier 3 buildings is depicted in Figure 5.
- Asset analysis: MSA analysis is performed for each asset considering all potential hazards affecting it to define its fragility curves.

- Hazard analysis: all stressors to which the assets are sensitive are considered and the relationship between the severity of the excitation and the frequency with which each level of excitation is exceeded, is defined.
- Loss analysis: the vulnerability function is defined for each asset given the environmental stressor intensity as measured by the pertinent IM. Vulnerability functions describe the distribution of a loss measure given the level of the IM. The loss is quantified in terms of repair cost, downtime and functionality.
- Decision making: the results of risk assessment help authorities and decision makers from CH and non-CH assets stakeholders to establish prioritization protocols and to manage associated incidents, facilitating the rapid assessment of the state of the assets.

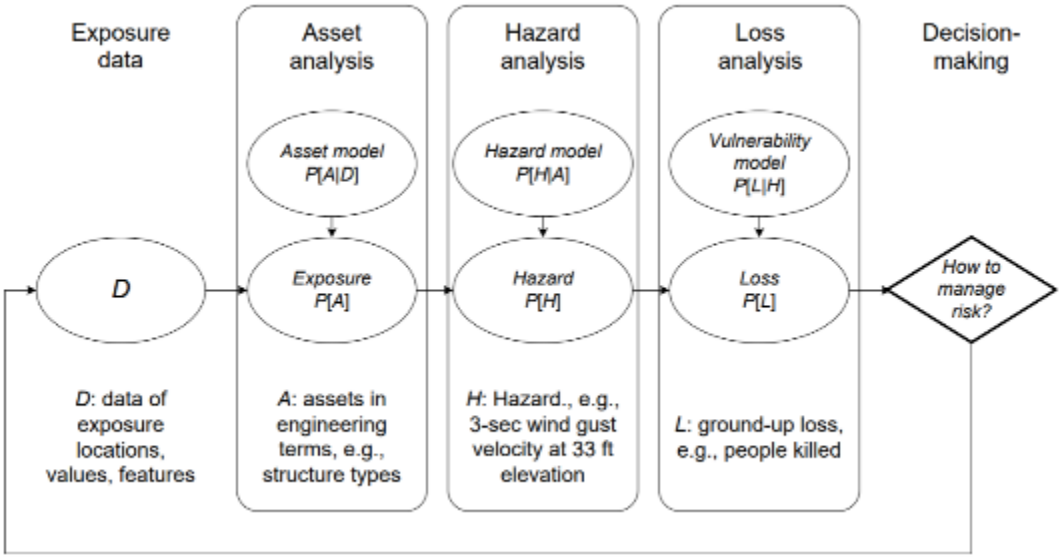

Figure 4: Natural catastrophe risk analysis framework (Porter 2019).

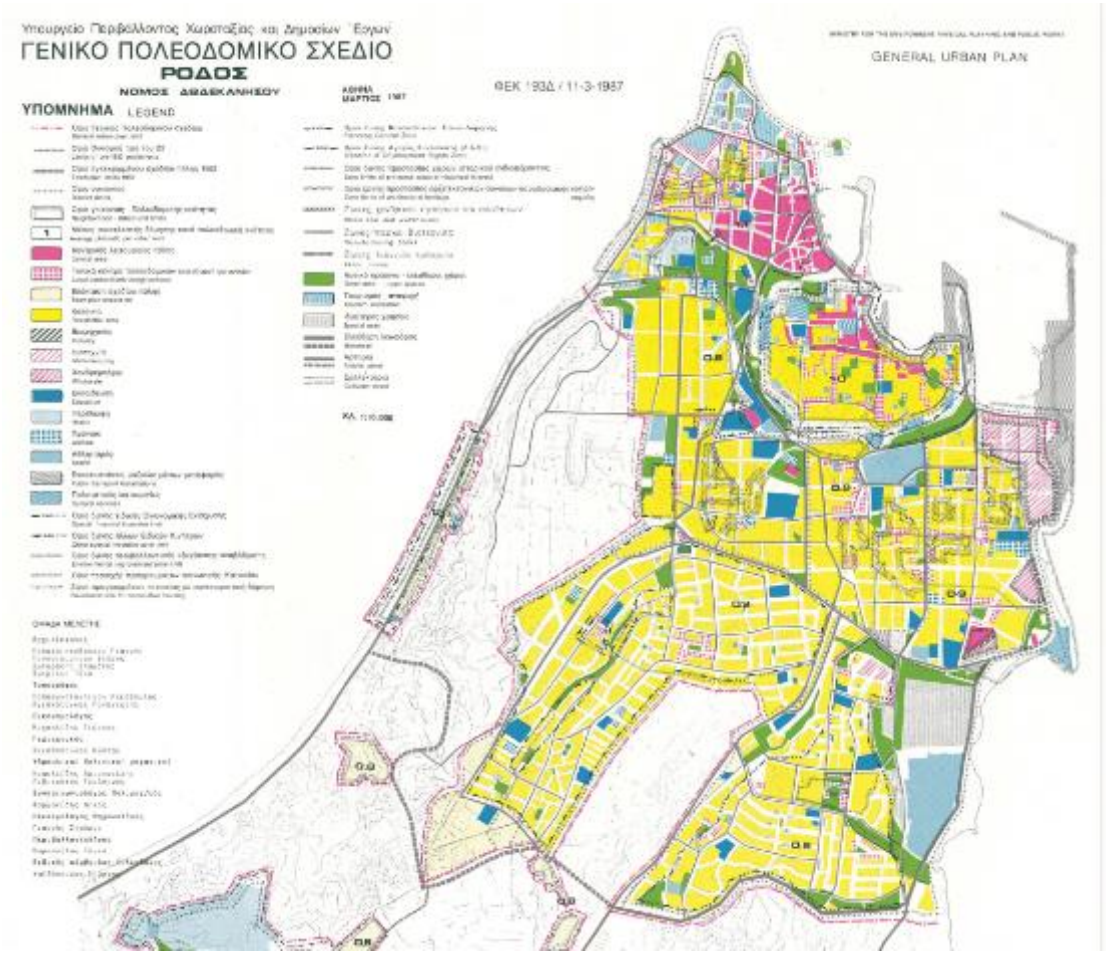

Figure 5: Rhodes general urban plan.

2.3.1 Fragility functions

The continuous damage measure (*DM*) is discretized into a finite number of *N* damage states DS_i (*i* = 0...*N*-1), separated by *N*-1 associated limit-states LS_i, *i* = 1…*N*-1. This way, fragility curves arise naturally and each one is a continuous function that provides the probability of exceeding a given LS_i, or equivalently of being in DS_i or worse, given the IM. A fragility function is defined by the expression:

$$F_{LSi}(IM) = F_{LSi}(IM = x) = P\left[LS_i \text{ violated} \mid IM = x\right] = P\left[D > C_{LSi} \mid IM = x\right] \quad (2)$$

where limit state LS_i violation is typically defined as the seismic demand, *D*, exceeding the associated limit-state capacity, C_{LSi}. Typically, fragility curves are assumed to follow the lognormal distribution. If ϑ_i is the median value and β_i is the logarithmic standard deviation (or dispersion) of DS_i, the probability of exceeding DS_i is computed as follows:

$$F_{LSi}(IM) = F_{LSi}(IM = x) = \Phi\left(\frac{\ln(x/\theta_i)}{\beta_i}\right) \quad (3)$$

where $F_{LSi}(IM)$ is the probability of exceeding DS_i given $IM = x$ and $\Phi(\cdot)$ denotes the standard normal cumulative distribution function.

Damage states can be sequential, mutually exclusive or simultaneous. Sequential damage states are the norm and they occur one after the other, with DS_{i+1} always succeeding DS_i, as damage increases in the structure and more severe consequences occur. Sometimes, one of the DS_i may be defined as a mutually exclusive or simultaneous occurrence of two or more higher-detail damage states. The occurrence of one damage state precludes the occurrence of the other for mutually exclusive *DS*, which is typical of components following one or another failure mechanism (but not both). Simultaneous *DS* may occur at the same time, which is typical of different components in a complex subsystem that may receive damage simultaneously (e.g., the cabin and counterweight of an elevator). In Figure 6 an example of the fragility curves of three sequential damage states is presented. The probability of being in each damage state for sequential damage states is estimated as per Eq. (4) and indicated by the black arrowed lines in the same Figure.

$$P(in\,DS_i \mid IM) = F_{LSi+1}(IM) - F_{LSi}(IM) \tag{4}$$

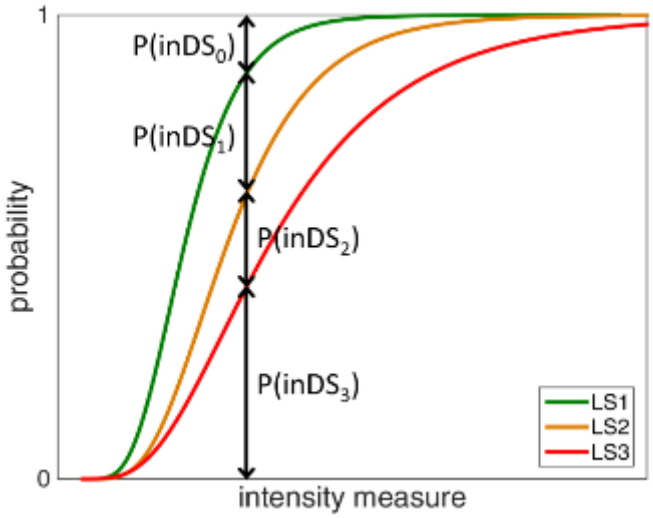

Figure 6: Fragility curves for three sequential limit states. The black arrowed lines indicate the probability of being in each damage state for a certain IM value.

The most comprehensive analytical methods for fragility assessment rely on advanced numerical models subjected to nonlinear dynamic analyses. In HYPERION multi-stripe analysis is employed for analysing the response of the assets. Given the EDP threshold values for the structure, the fragility curves are calculated through MSA results. Each curve corresponds to a single limit state, as indicatively shown in Figure 7.

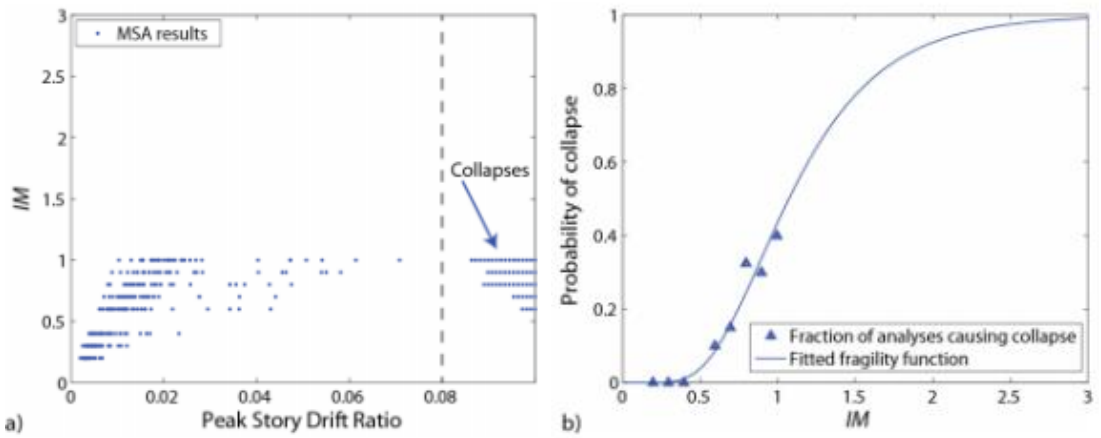

(a) (b)

Figure 7: (a) Example of MSA results and (b) discrete versus fitted collapse fragility function (Baker 2015).

2.3.2 Vulnerability functions

Vulnerability functions are probabilistic distributions that are used to "convert" the physical damage of the structure to monetary loss, repair time, downtime, etc., given the level of IM. The vulnerability functions can either be derived directly or analytically. In the former case, empirical methods are employed by considering losses from past events at given locations with the IM of the event, while, in the latter case, vulnerability functions are derived from the combination of fragility and consequence functions (empirically derived probabilistic distributions of losses given a performance level). The analytical estimation procedure of vulnerability functions is schematically depicted in Figure 8. The consequence functions are probabilistic distributions of losses, given a performance level, that are mainly derived empirically.

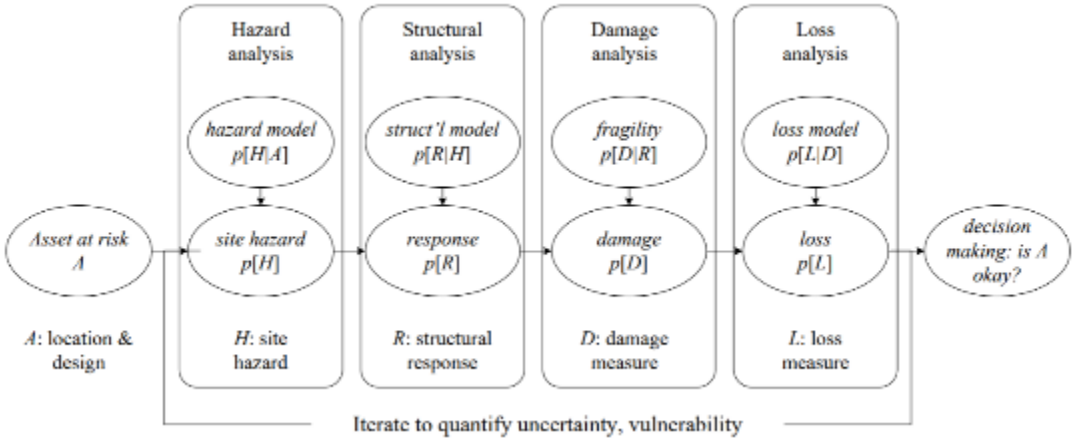

Figure 8: Framework for analytical estimation of vulnerability of a single asset (Porter 2019).

Within the HYPERION platform, two approaches are used to define CH and non-CH assets' vulnerability curves:

Component-based vulnerability assessment approach

The approach of FEMA P-58 (ATC 2009) is adopted, where vulnerability functions are obtained by correlating asset EDPs directly to loss. This process requires detailed information regarding the fragility and loss functions on all vulnerable components of each asset. The mean vulnerability function per component category, the behaviour of which is controlled by EDP_i, is calculated as:

$$E(L_i \mid EDP) = N_{i,h} \sum_{i=0}^{N_{ds}} P\left(ds_i \mid EDP\right) \cdot m_{i,ds} \tag{5}$$

where i is an index to the component category, L is the loss, N_{ds} is the number of possible component damage states, $N_{i,h}$ is the quantity of components of category i in group h and $m_{i,ds}$ is the mean loss per unit of component category i in damage state ds.

System-only vulnerability assessment approach

In this approach the vulnerability functions are obtained by convolving system-level fragility curves with the corresponding cumulative cost/consequences of an asset's damage state i, DS_i. The mean vulnerability curve is calculated according to Eq. (6):

$$E(L \mid IM) = \sum_{i=0}^{N_{DS}} E(L \mid DS_i) \cdot P\left(DS_i \mid IM\right) \tag{6}$$

where N_{DS} is the number of damage states, $P(DS_i \mid IM)$ is the probability of being in damage state i given the IM, $E(L \mid DS_i)$ is the expected loss (e.g. cost/downtime etc.) given DS_i and $E(L \mid IM)$ is the expected loss given the IM. An example of vulnerability curve estimation using deterministic loss data is schematically shown in Figure 9. The variance, $var(L \mid IM)$, of the vulnerability curve is obtained according to Eq. (7):

$$\mathrm{var}(L \mid IM) = \sum_{i=0}^{N_{DS}} \left[\mathrm{var}(L \mid DS_i) + E^2(L \mid DS_i) \right] \cdot P\left(DS_i \mid IM\right) - E^2(L \mid IM) \tag{7}$$

The vulnerability curves can be obtained by repeating the process presented above with Eqs. (6) and (7) for a range of IMs. Indicative results are portrayed in Figure 10 where the median and 16% and 84% quantiles of the vulnerability function are shown.

Comparison of the approaches

There is a considerable difference between these two approaches for estimating the vulnerability function. In the first one (FEMA P-58 approach), the asset is examined on a component basis regarding the damages and the consequences. Thus, for example, a CH sustaining DS_2 in the façade is distinguished from one sustaining DS_2 in its roof. The first one can be seen as a catastrophic failure, while the second one may be considered as more easily repairable. Then, in the second approach (system-only vulnerability), the entire system, namely the entire CH or non-CH asset, is characterized by a single DS leading to a coarse resolution regarding the determination of consequences.

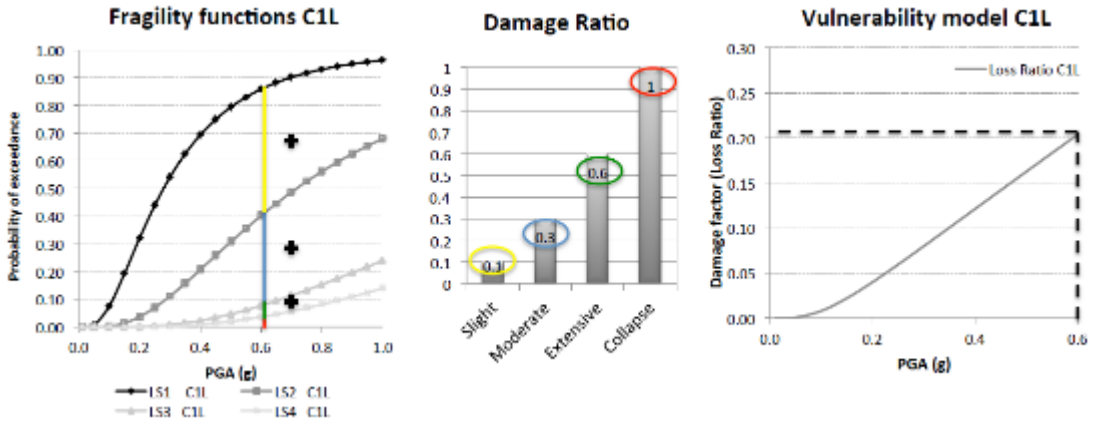

Figure 9: Example of vulnerability assessment given fragility and deterministic consequence data (D'Ayala et al. 2015).

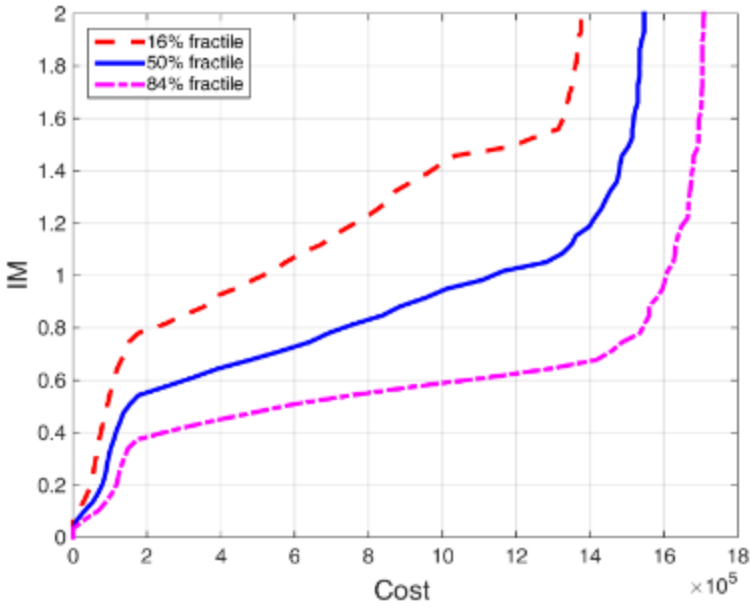

Figure 10: Mean, 16% and 84% quantiles of vulnerability curves in terms of cost computed using probabilistic cost distributions.

2.4 Materials deterioration

Several types of materials comprise the CH of the pilot cities, such as rammed earth, brick masonry, stone (limestone) masonry or timber. In this section, a description of the on-going work on material degradation characterization and its inclusion in MHVMs is presented.

2.4.1 Rammed earth

Rammed earth construction is an ancient technique, carried out by compacting layers of rammed earth. Granada (Spain) comprises several rammed earth sites such as the outer walls of the Alhambra Palace and many Moorish houses within the Albaicín area (UNESCO World Heritage from 1994).

With respect to the mechanical properties of rammed earth, this section describes the manufacturing of the rammed earth samples, and the testing procedures for evaluating their compressive strength. The earth material used in the Hyperion project was taken from an existing quarry located 45 km from the city of Granada. Figure 11 shows the quarry and the pertinent material.

Figure 11: Quarry in the Granada region of Spain.

In order to determine the water content for optimum compaction, the standard Proctor test procedure, according to the Spanish Standard (UNE 103-500-94), was followed. A range of water content (7%-12%) was selected to obtain the maximum dry density. It is observed from Figure 12 that the optimum water content for preparation of rammed earth was 8% by mass.

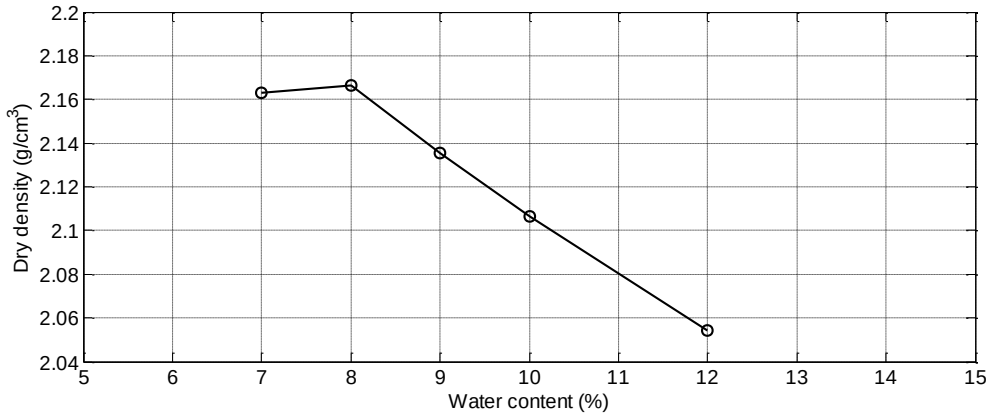

Figure 12: Results of the Standard Proctor test.

The earth material was mixed with the optimum water content (8% by mass), and a cylindrical mold was used to prepare the samples. There were six compaction layers in each specimen. The Proctor energy (E=0.583 J/cm^3) was measured with a manual rammer. Each compacted layer had a thickness of about 5 cm and consisted of 2 kg of earth material. In Figure 13 the manufacturing process of the rammed earth samples is presented.

Figure 13: Sample manufacturing of rammed earth.

The samples were left drying for 4 months, and, subsequently, the uneven surfaces were capped with a thin layer of cement mortar to get a smooth and flat end surface. Next, an unconfined compressive strength test was done with a loading speed of 0.05 mm/s and is depicted in Figure 14.

Figure 14: Unconfined compressive strength test of rammed earth.

The obtained strength-strain results are presented in Figure 15, with the average compressive strength being 0.7987 MPa.

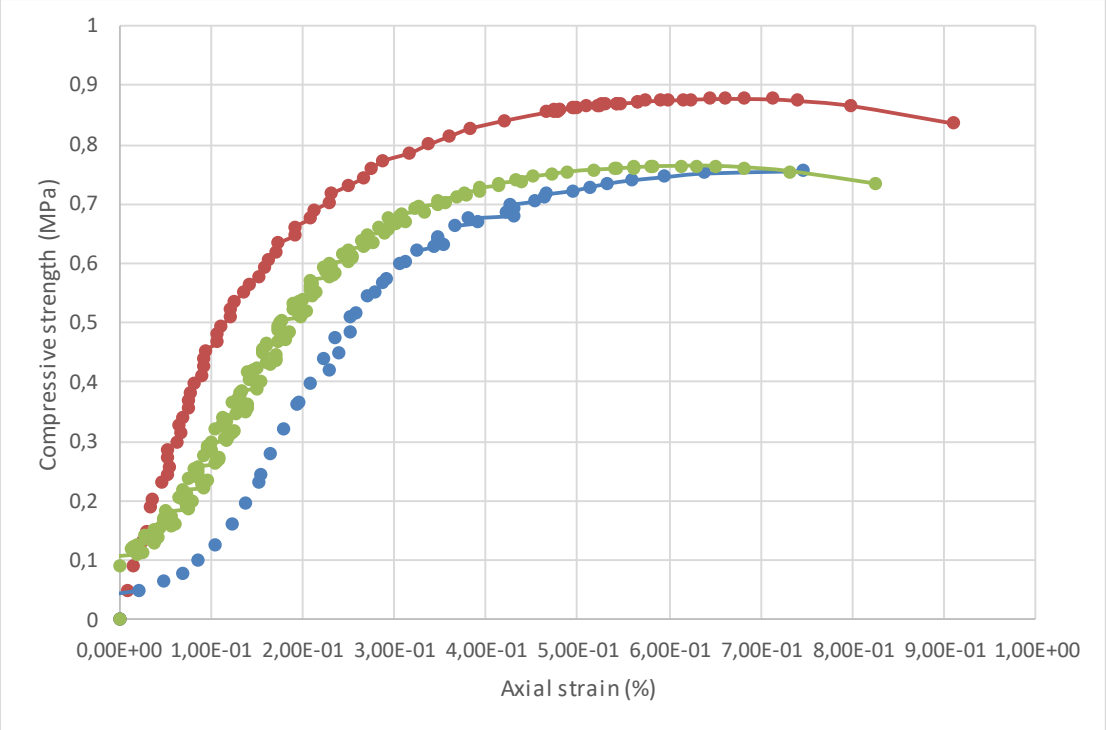

Figure 15: Results of the unconfined compressive strength test of rammed earth.

2.4.2 Brick masonry

The analysis of decay in brick masonry often reveals an uneven distribution of the deterioration patterns, determined by the heterogeneity of the building materials, and the localised effects of the deterioration agents, and resulting in significant differential recession of the bricks (Figure 16).

Figure 16: Example of differential brick masonry decay. Images from the external walls of the Arsenal in Venice.

Besides the negative aesthetic consequences, severe differential material loss from brick walls may result in significant reduction of wall thickness and, eventually, structural issues in brick masonry. In order to contribute to the vulnerability assessment, it is important to quantify the already occurred loss, map the

deterioration patterns, and recognise the critical environmental factors and specific petrographic features of the bricks that determine the different behaviour of neighbouring bricks.

For this reason, selected Tier 2 buildings are under investigation, in order to determine the amount and distribution of material loss from 3D reconstructions of the surface topography, obtained by photogrammetry and/or laser scanning, as well as the distribution of the deterioration patterns. When possible, samples will be collected for mineralogical-petrographical characterisation, in order to determine whether differences in recession rate are related to specific compositional, textural and technical features, as a result of heterogeneity in the manufacturing process (e.g. with reference to the nature and proportions of the different raw materials or to the firing conditions).

This will allow a classification of the different elements of brick masonry with respect to the distribution of the deterioration patterns, and the specific petrographical and textural properties. This data will feed fragility and vulnerability functions within a general performance assessment framework for that specific cultural asset.

2.4.3 Stone masonry

Seven of the twelve rock types selected (Table 2) were analysed from a physical and mechanical point of view. Porosity (open porosity, P_o, in %) and density (bulk and skeletal densities, ρ_b and ρ_{sk}, respectively) were determined by Mercury Intrusion Porosimetry (MIP) on a Thermo Scientific Pascal 140-240 apparatus on freshly cut samples of approximately 1.5 cm^3.

Table 2: Stone samples, origin and labels.

	Origin	Lithology	Rock type	Label
ROCK SAMPLES	Italy	Red Verona	Nodular limestone	RV
		Botticino Stone	Limestone	BL
		Istria Stone	Limestone	IS
		Costozza Stone	Soft Limestone	CS
		Carrara Marble	Marble	CM
		Trachyte	Effusive rock	ETr
	Norway	Syenite	Intrusive rock	TSy
		Rhyolite	Effusive rock	TRh
	Spain	Macael Marble	Marble	MM
		Santa Pudia	Limestone	GSP
	Rhodes	Sfouggaria Stone	Limestone	SS
		Lartios Stone	Limestone	LS

Elastic-mechanical characteristics and structural anisotropy of stones were measured by non-destructive tests using ultrasonic waves velocities. Ultrasonic waves were transmitted using an EPOCH650® Ultrasonic Flaw Detector (Olympus) in the three

perpendicular directions of the samples. Measurements were performed with transducers of 0.5 MHz over a circular contact surface of 3 cm in diameter. A viscoelastic couplant (an ultrasound eco-gel) was used for effective coupling between the transducers and the sample surfaces.

The propagation velocities V_{p1}, V_{p2} and V_{p3} (compression pulses, Figure 17) were measured along the three perpendicular directions of the cube-shaped samples (50-mm edge, Figure *18*) to determine structural anisotropies (Molina et al., 2013) as follows:

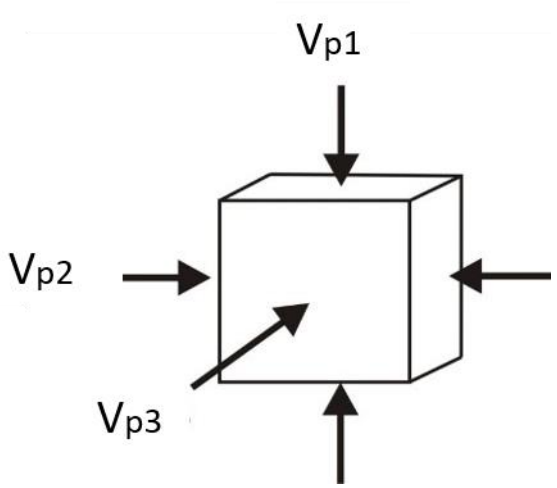

Figure 17: A scheme of the propagation velocities V_{p1}, V_{p2} and V_{p3} (compression pulses) along the three perpendicular directions of a cube-shaped sample.

Total Anisotropy (ΔM) = (1- $\frac{2V_{p1}}{V_{p2}+V_{p3}}$) x 100;

Relative Anisotropy (Δm) = $\frac{2(V_{p2}-V_{p3})}{V_{p2}+V_{p3}}$ x 100;

where V_{p1} = max propagation velocity, V_{p2} = mean propagation velocity, and V_{p3}= min propagation velocity.

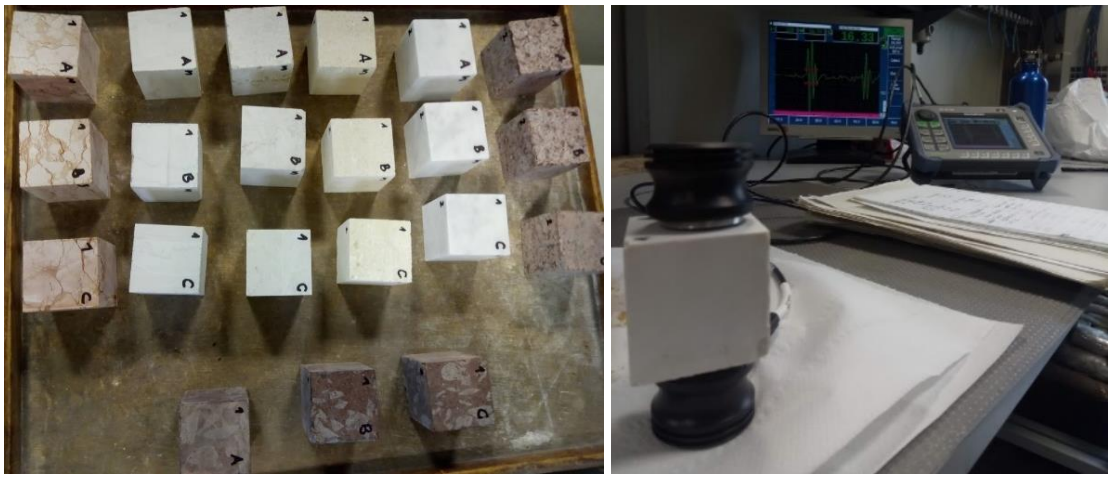

Figure 18: Left: Cube-shaped stone samples. Right: Ultrasonic Test performed on a sample of Carrara marble.

Poisson's Coefficient (ν), Young (E), shear (G) and bulk (K) modules were calculated from the measured average wave velocities V_p and V_s (shear pulses) propagation velocities as follows (Molina et al., 2013):

Poisson's Coefficient (ν) = $\frac{(\frac{V_p}{V_s})^2-2}{2\,[(\frac{V_p}{V_s})^2-1]}$; Young's Modulus (E) = $2\rho_b V_s^2\,(1+\nu)$;

Shear Modulus (G) = $\frac{E}{2(1+\nu)}$; Bulk Modulus (K) = $\frac{E}{3(1-2\nu)}$;

where ρ_b is the bulk density (Kg/m^3) (according to values determined by MIP).

Table *3* below shows the summary of results obtained for the physical and elastic-mechanical parameters. Some data have been integrated from literature.

Table 3: Mercury Intrusion Porosimetry (MIP): ρ_b = bulk density (Kg/m^3); ρ_{sk} = skeletal density (Kg/m^3); P_o = open porosity (%). Ultrasonic Test (UT): V_{p1} = max propagation velocity; V_{p2} = mean propagation velocity; V_{p3} = min propagation velocity; ΔM = Total anisotropy; Δm = Relative anisotropy; V_p = average compressional propagation velocity of ultrasonic pulses; V_s = average shear propagation velocity of ultrasonic pulses; ν = Poisson's ratio; E = Young's modulus (GPa); G = shear modulus (GPa); K = bulk modulus (GPa). Uniaxial Compressive Strength test (UCS, data from literature): σ = mechanical stress (MPa).

	RV	**BL**	**IS**	**CS**	**CM**	**ETr[1]**	**TSy**	**TRh**	***MM*[2,3]**	***GSP*[4]**	***SS*[5]**
ρ_b	2693	2740	2711	2448	2707	2380[1]	2720	2649	*2500-2750*[2]	*1725*[4]	*2450*[5]
ρ_{sk}	2695	2748	2713	2741	2719	2640[1]	2745	2671	-	*2616*[4]	-
P_o	0.08	0.29	0.09	28.95	0.46	11.16[1]	0.455	0.82	*0.1-0.6*[2]	*32.8*[4]	*18.7*[5]

V_{p1}	4923	5381	5607	3047	5574	-	4777	5233	*5165*[3]	-	-
V_{p2}	5189	5566	5679	3209	5643	-	4824	5301	*6573*[3]	-	-
V_{p3}	5298	5697	5758	3355	5734	-	4986	5391	*6597*[3]	-	-
ΔM	6	4	2	7	2	-	3	2	*21.56*[3]	*3*[4]	-
Δm	2	2	1	4	2	-	3	2	-	*9*[4]	-
V_p	5137	5548	5681	3204	5651	-	4862	5308	-	*3593*[4]	-
V_s	2919	3052	3076	2056	3105	-	2874	3030	-	*1730*[4]	-
ν	0.26	0.28	0.29	0.15	0.28	-	0.23	0.26	-	*0.35*[4]	-
E	58.66	66.37	67.21	22.64	67.91	-	56.08	62.03	-	*14.11*[4]	-
G	23.25	25.87	26.00	9.84	26.45	-	22.77	24.65	-	*5.23*[4]	-
K	40.99	50.96	53.99	10.78	52.32	-	34.81	42.78	-	*15.59*[4]	-
σ	-	183[6]	-	-	101.4[6]	-	-	-	*81.1-87.4*[2]	*11*[4]	-

Data from Germinario et al. (2017) (quarry of Mt. Merlo, NE Italy), Navarro et al. (2013), Luque et al. (2011), Molina et al. (2013), Avdelidis et al. (2003), and Salvini PhD Thesis (2017).

Hereafter, the work done is focused on experimental analysis to characterise the local limestone from Granada, and Bayesian methods to identify the most likely degradation pattern in CH stone buildings using photogrammetry data.

- Experimental analysis

Limestone is widely used in Granada (Spain). With respect to its mechanical properties, this section describes the testing procedures for evaluating their compressive strength.

Some samples were obtained from “Los Linos” quarry, 25 km from Granada. The samples were cubic, each side being 120 mm, as it is observed in Figure *19*.

Figure 19: Samples of limestone.

The unconfined compression test of the samples was done with a loading speed of 0.05 mm/s. The test set-up and the obtained strength-strain results are presented in Figure 20 and Figure *21*, respectively. The average compressive strength was 3.401 MPa, with a standard deviation of 0.0825 MPa.

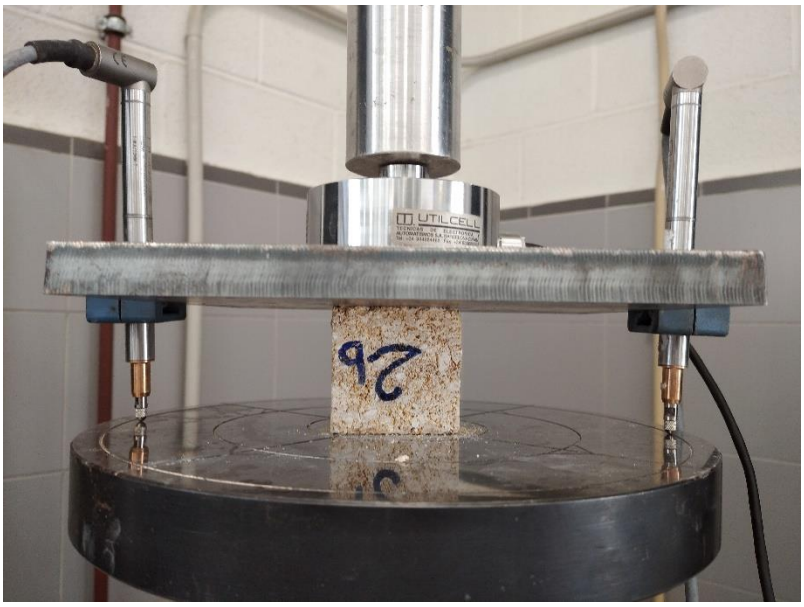

Figure 20: Unconfined compressive strength test of limestone.

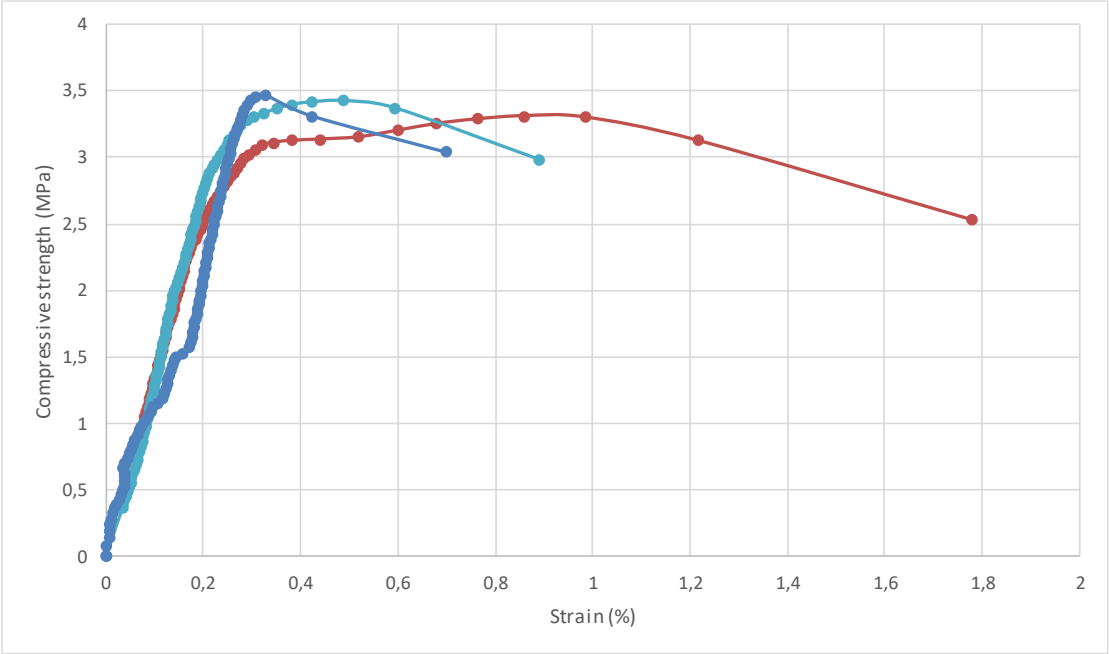

Figure 21: Results of the unconfined compressive strength test of limestone.

- Degradation patterns

A probabilistic Bayesian method is proposed (Jalón et al., 2020) to identify the most plausible degradation pattern using photogrammetry data. The methodology is applied to the San Jerónimo Monastery (Figure 22), a CH building in Granada (Spain), classified as Tier 1.

Figure 22: Main facade of San Jerónimo Monastery.

As an example, the main facade is analyzed by adopting three candidate degradation patterns: Bilinear, Triangular, and Square. In Figure 22, the measured degradation profiles (S1, S2) of the main facade, the different candidate degradation patterns and their confidence intervals are presented. The heterogeneity and complexity of the measured degradation profiles are noteworthy.

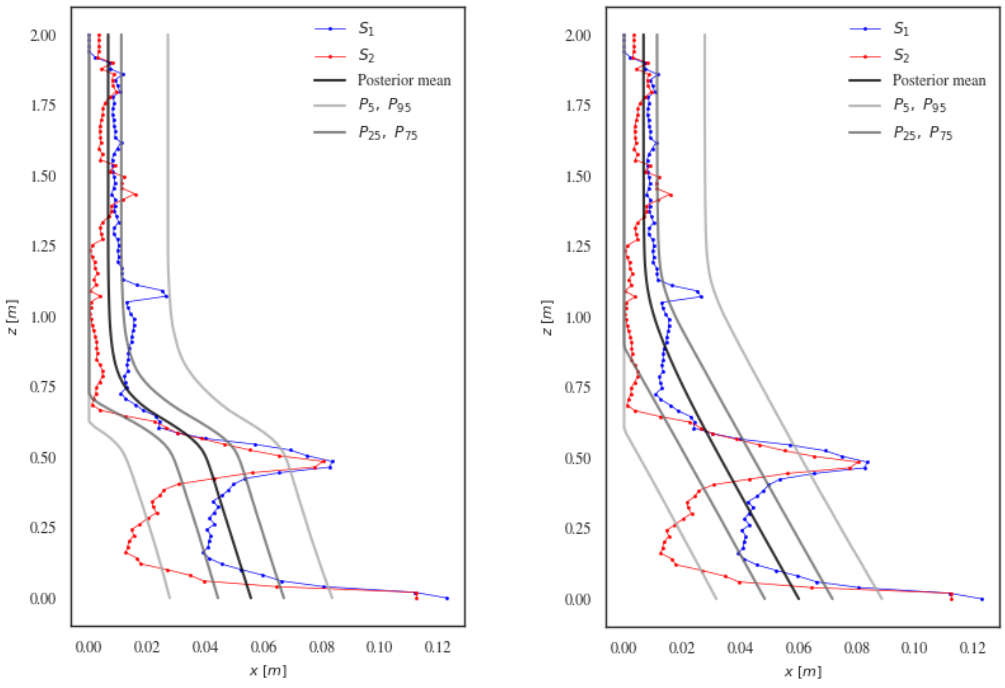

a) b)

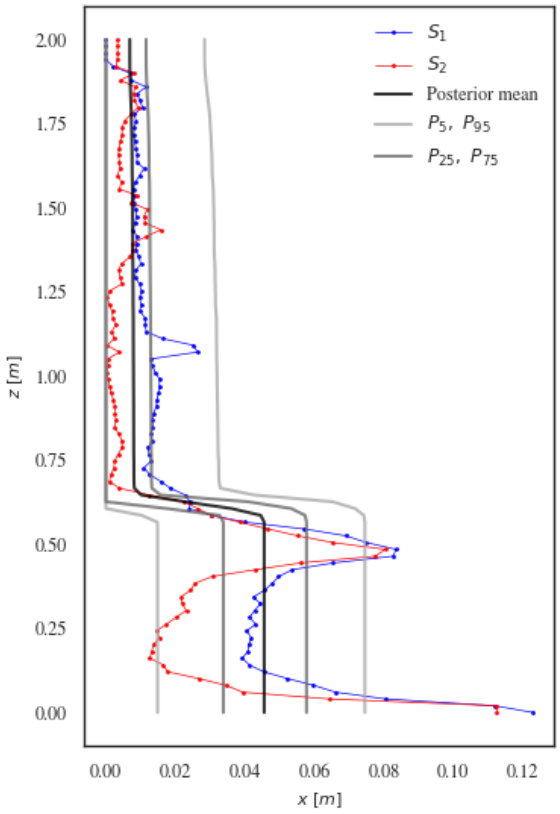

c)

Figure 23: Measured degradation profiles (S_1, S_2), posterior mean degradation pattern, and confidence intervals (P_5, P_{25} , P_{75}, P_{95}) – a) Bilinear model, b) triangular model, c) square model.

Next, the relative likelihood of the candidate degradation patterns are computed following the methodology explained in Jalón et al. (2020). The results are shown in Figure 24. Note that the Bilinear Model is shown to be the most suitable (P=0.968) to estimate the degradation of the main facade.

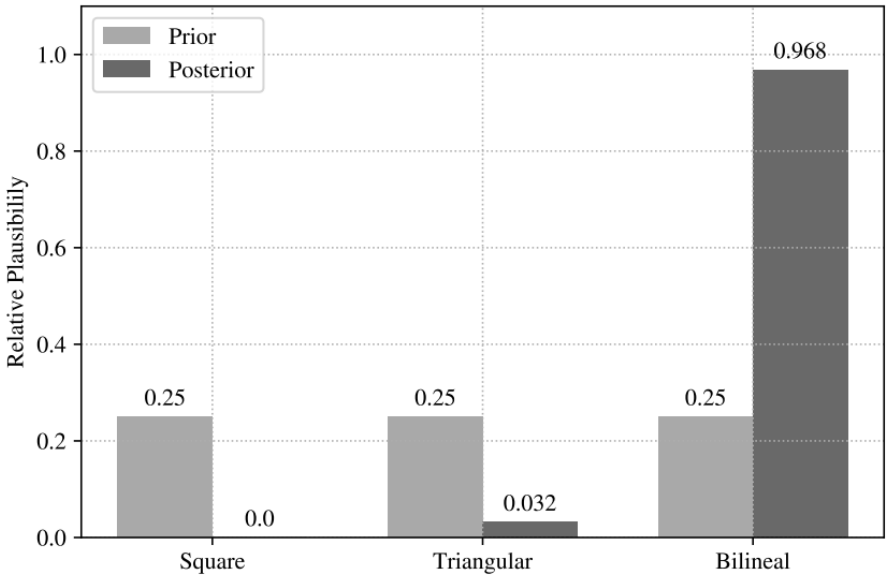

Figure 24: Degradation pattern ranking.

2.4.4 Timber

Timber is a construction material widely used in Norway. The CH buildings selected for the Hyperion project made of timber are presented in Table 11. The timber CH buildings are sensitive to degradation caused by biological factors (e.g., termites, decay fungi, etc.), climate-related conditions (e.g., snow, rain, flood, landslide, etc.) and man-made hazards (e.g., fire). The decay process usually decreases the cross section, subsequently affecting its structural safety.

In order to carry out the vulnerability assessment, it is important to quantify the actual loss of material and map the deterioration patterns, recognise the critical environmental factors and the specific mechanical features of the timber, to support informed decision-making about a possible decommissioning (for non-CH buildings), or level of repair and lifespan extension.

3 Applicable assets

In HYPERION three tiers are envisioned: Tier 1, Tier 2 and Tier 3. In more detail:

- **Tier 1**: A CH building of high importance for the area where there are already existing monitoring sensors or a permission can be obtained for the installation of sensors for the purposes of the project. For this building detailed modelling will be provided. Tier 1 assets are influential CH structures that require structure-specific treatment. For these, detailed and/or reduced-order models are created to offer a comprehensive understanding of their response. Detailed models are good for considering issues of corrosion, localized damage and thus correlating with sensor information. They are not very useful for propagating uncertainty and performing assessment due to their considerable computational expense. Thus, simpler models with a low number of degrees of freedom are employed to conduct dynamic analyses for the Tier 1 assets. Performance assessment for the Tier 1 assets is performed by employing asset-specific fragility and vulnerability functions. Tier 1 assets are treated on a component-basis because it allows differentiating the damage and consequences to individual asset components; thus, it enables a more detailed assessment.
- **Tier 2:** Two types of buildings are included in this category. The first one is a CH structure of high importance for the area where it is not possible to install sensors, due to either permission issues, cost, or availability. The second type includes buildings that are non-CH structures but very important for the Business Continuity of the area, such as fire houses, hospitals and airports. As in Tier 1, for structures in Tier 2 category detailed and/or reduced-order models are created to offer a comprehensive understanding of their response. Also, performance assessment for the Tier 2 assets is performed by employing asset-specific fragility and vulnerability functions.
- **Tier 3**: All vulnerable CH and non-CH assets that will be modelled/studied within the scope of the project and do not receive an asset-specific (i.e., Tier 1 or 2) treatment fall in the category of Tier 3. Such assets receive a low-resolution class-specific (or asset-agnostic) treatment, by categorization into broad classes of a taxonomy distinguishing salient macro characteristics of each structure (e.g., age, material, structural system type, etc.) but not detailed asset-specific ones. Consequently, the fragility/vulnerability approach adopted for risk assessment purposes is the system-only one, which is less detailed, thus the damage and consequences are evaluated directly for the entire asset rather than its individual components.

The performance assessment approach adopted for each tier is listed in Table 4:

Table 4: Asset categories in HYPERION, their specificity and preferred fragility/vulnerability approach.

Asset category	Specificity	Preferred vulnerability approach	Sensor integration
Tier 1	Asset-specific	Component-based	Yes
Tier 2	Asset-specific	Component-based	No
Tier 3	Class-specific	System-only	No

The procedure of FEMA P-58, presented in Figure 25, is followed for the performance assessment of all assets. Multiple potential scenarios that may happen on each asset are generated. For instance, regarding the assets treated via a component-based approach, for each IM scenario the component's EDPs are determined based on the multi-stripe analysis results (that are stored in the *name*.msa.mat/xml file). By convolving the fragility functions of each individual component with the associated consequence functions (stored in *name*.mtdata.mat/xml file), multiple IM-DV (or intensity-to-consequences) scenarios are generated. Note that for each IM scenario, if the asset has not collapsed, the consequences are calculated based on the aggregated damage and associated consequences sustained by each component. If the asset has collapsed, the consequences for replacing the asset are considered using global fragility and consequence functions. A similar methodology is followed for the performance assessment of assets that receive a system-only treatment, by employing system-only global fragilities and consequence functions instead of component-based ones.

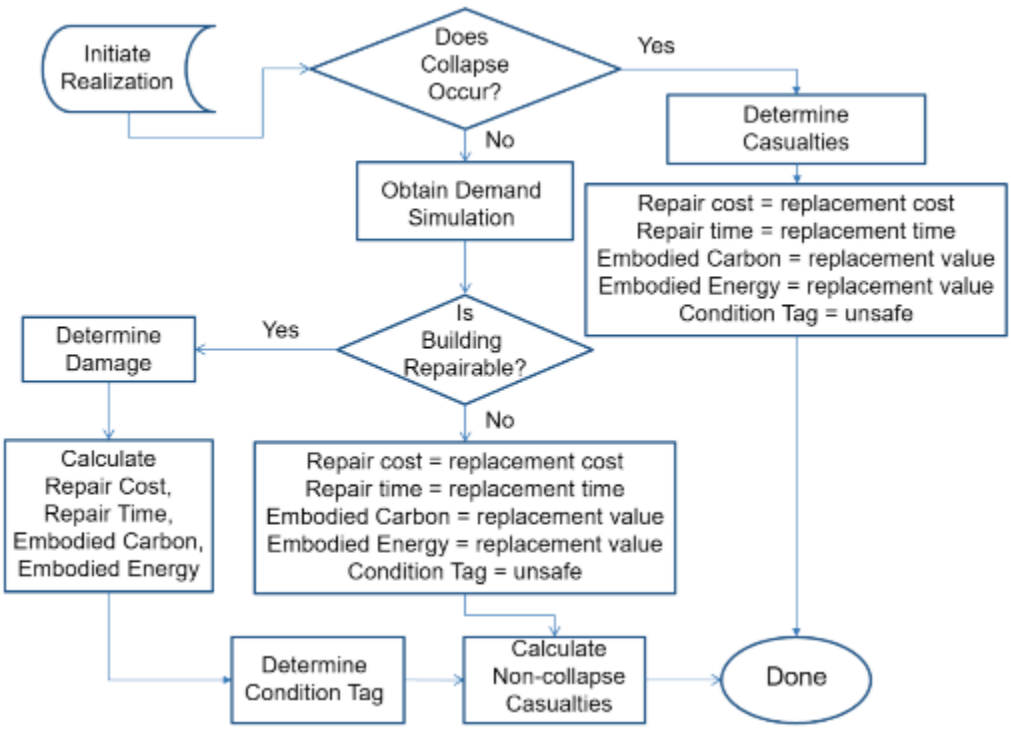

Figure 25: Flowchart for performance calculation (FEMA P-58).

Consequently, by processing the data stored in scenario MSA and metadata files of each asset, multiple potential damage/consequence scenarios are generated given all potential hazards. By combining this information with the IM fields, which describe the spatial distribution of the hazard, "all" potential scenarios that may happen on the portfolio of CH and non-CH assets are generated.

The assets of each test site are classified as either CH or non-CH. The CH assets are distinct self-contained parts of the city, such as bridges, archaeological sites, tower, monasteries, etc. The non-CH assets are structures indirectly related or affecting the overall city and community built around the CH area, e.g. residential and commercial buildings, antennas, powerlines, fire stations, hospitals, public administration buildings, etc.

3.1 CH assets

A brief description and categorisation of example CH assets is presented. More details on CH assets can be found in Deliverable D2.3 (Zeppos et al. 2019).

3.1.1 Masonry towers, fortifications, and bridges

Towers and fortresses constructed with various materials, during different periods and suffering different level of material degradation and damage are examined. CH structures falling in this category are presented in Table 5 for Granada, Table 6 for Rhodes, Table 7 for Venice, and Table 8 for Tønsberg.

Table 5: Granada CH towers, fortresses and bridges

Asset	
Puerta Elvira (fortress)	

Table 6: Rhodes CH towers, fortresses and bridges

Asset	
Saint Nikolas lighthouse and fort	
Nailac Pier	
The Roman bridge	

Table 7: Venice CH towers, fortresses and bridges

Asset	
Torre dell'Orologio	
Rialto bridge	
Ponte della Libertá	

Table 8: Tønsberg CH towers, fortresses and bridges

Asset	
Stottsfjell Tower	

3.1.2 Timber and unreinforced masonry buildings

Buildings are typical CH assets, which in some cases are still in use, such as the San Jerónimo Monastery in Granada, or the fire station, the police station and the City Hall in Rhodes. The CH buildings examined in each test site are presented in Table 9 for Granada, Table 10 for Rhodes, for Tønsberg, and in Table 12 for Venice.

Table 9: Granada CH buildings

Asset	
San Jerónimo Monastery	

The mill of the Marquis of Rivas	

Table 10: Rhodes CH buildings

Asset	
Fire station	
Police station	

S. Aegean Regional building	
Municipality of Rhodes (City Hall)	
Central offices of Ephorate of the Dodecanese islands	

Table 11: Tønsberg CH buildings

Asset	
The Heierstad Loft	
The Fadum Store house	
Bentegården	

Table 12: Venice CH buildings

Asset	
Ca' Pesaro Palace	
Buildings from *Piazzale Roma* to the Accademia bridge	
Civil Hospital	

3.1.3 Sites on the Countryside

Apart from towers, fortresses, buildings, etc, CH geo-sites are also examined in some test cities, such as the Grave enclosures in Rhodini, Rhodes (Table 13) and the area of the ruins of the Western Tower in Tønsberg (Table 14).

Table 13: Rhodes CH sites on the countryside

Asset	
Grave enclosures in Rhodini	

Table 14: Tønsberg CH sites on the countryside

Asset	
Western Tower	

3.2 Non-CH assets

3.2.1 Buildings

Non-CH buildings considered to be Tier 2, plus some Tier 3 ones, are critical for the functionality of a city, affecting the business continuity and the financial sustainability of the study area. In Rhodes, for example, these buildings are the Electrical Power Substation, the Public Services building, the Regional Hospital (Figure 26), and the airport (Figure 27).

Figure 26: Rhodes regional hospital.

Figure 27: Main terminal building of Rhodes international airport.

Moreover, the building stock of an area in each test site is examined as Tier 3 buildings. In Rhodes, for example, the overall area that will be modelled/examined is the entire city that covers an area of approximately 1400km^2. This area is divided in sub-areas, based on the material and the year of construction, as illustrated in Figure 28.

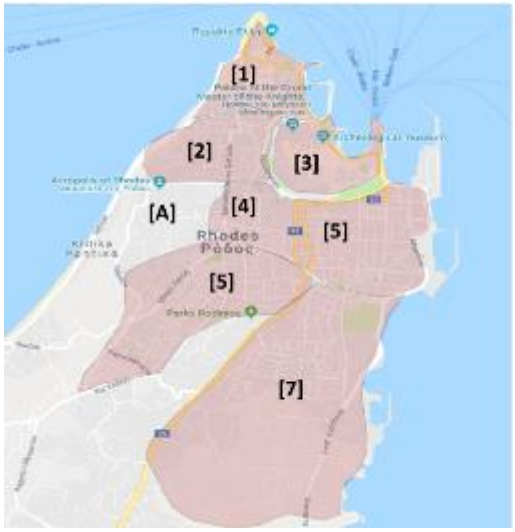

[A] : ancient part of city

[1] - [2]: city center with RC buildings, mixed commercial and residential areas

[3]: wall surrounded Medieval City (UNESCO heritage site), mixed commercial and residential area, unreinforced masonry

[4] – [6]: suburban city with RC buildings, mixed commercial and residential areas, mainly after 1960

[7]: suburban city with RC buildings, mainly residential area, mainly after 2000

Figure 28: City of Rhodes: categories of building stock.

In Venice, the Ponte della Libertà viaduct connecting the historical center island to the mainland is an important non-CH Tier 2 asset, while the Marco Polo airport (Figure 29) and port (Figure 30) are classified as non-CH Tier 3 buildings. In addition, the industrial site of Porto Marghera is an important non-CH Tier 3 area to be modelled/examined. This industrial site is represented by a yellow line in Figure 31.

Figure 29: Venice, Ponte della Libertà (top), and Marco Polo Airport (bottom).

Figure 30: Venice Port.

Figure 31: Porto Marghera area, Venice.

In Granada, the fire station will be examined as non-CH Tier 2 structure (Figure 32), while Albayzín and Realejo areas (Figure 33) will be modelled/examined as Tier 3. The Albayzín area is the best-preserved illustration of a Hispano-Muslim city in Spain, enriched with the contributions of Christian Renaissance and Spanish Baroque culture.

Until 1990, the lack of global policy provoked the inadequate use of materials and techniques for some restorations. Nowadays, these defects are being rectified and reverted. Regarding the other historic area, Realejo was mainly a Christian expansion after Granada was reconquered. It owns many palaces and churches, mainly built with limestone and bricks, constantly being restored.

Figure 32: Fire house of Granada (Zeppos et al. 2019).

Figure 33: Map of Granada showing the Albayzin and Realejo areas (Zeppos et al. 2019).

Regarding the Tønsberg city, Figure 34 represents the selected area (4.01 km^2) for the survey, including all Tier 3 buildings, that are most influential within the Tønsberg municipality.

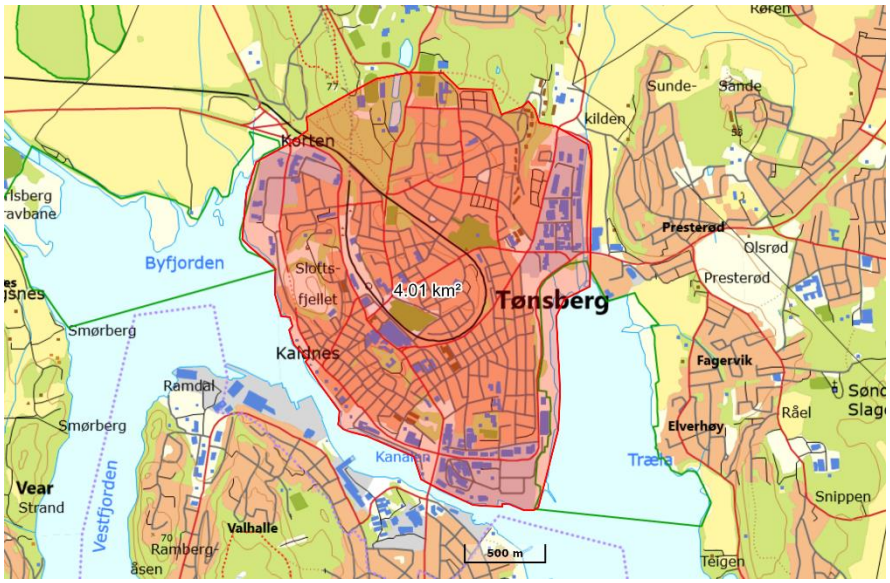

Figure 34: The Tønsberg study area.

3.2.2 Transportation network

The uninterrupted operation of the road network in case of a natural disaster is particularly important, especially in areas such as Rhodes island, where access to critical points, such as the airport, is not possible by different route alternatives. Thus, the assessment of the vulnerability of the road network under physical actions (e.g. earthquake, flood) is critical and necessary to continue the operation of the city. Critical parts of the transportation network of Rhodes are illustrated in Figure 35, as well as the Kremasti bridge on the main road linking the city to the airport. This bridge is highly affected by flooding as it only comprises a single lane serving a single direction, the other direction being served by a lane situated on the usually dry riverbed. Naturally, the elevated bridge lane needs to be used in turns when the riverbed is flooded.

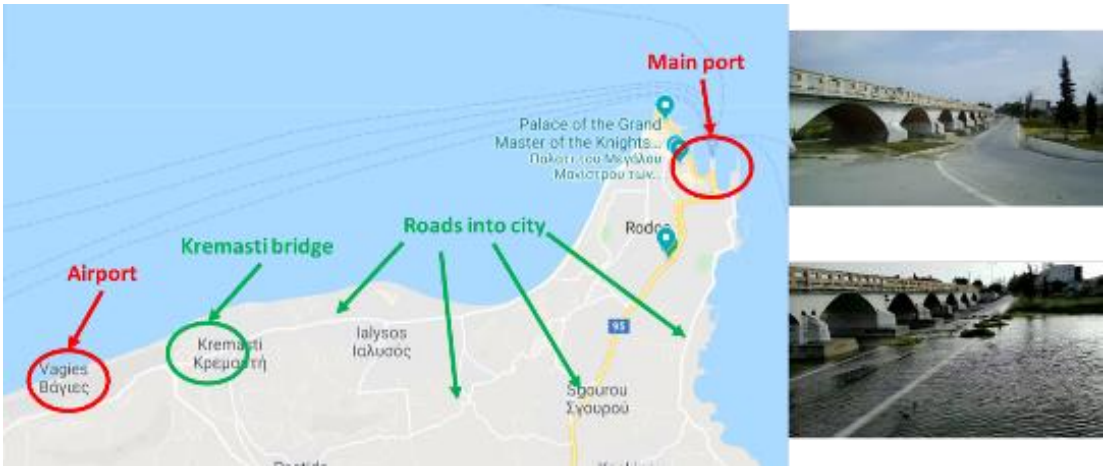

Figure 35: Left: Critical parts of the transportation network of Rhodes. Right: Flooding disrupting the access to the airport (Kremasti bridge).

3.2.3 Water and sewage network

The water supply and sewerage network of an area is a critical infrastructure whose integrity and efficient operation after a natural disaster is critical to the survival of the community. For example, the critical components of Rhodes water and sewage network are shown in Figure 36(a), while an illustrative example of water pipe failure is presented in Figure 36(b).

(a) (b)

Figure 36: (a) Critical components of Rhodes' water and sewage network, (b) failure of water distribution lines.

3.2.4 Power transmission and distribution network

The critical components of the electric power transmission system are the power transmission lines, the substations, the power control building, and the power distribution network (Figure 37). Power transmission lines form the high-voltage power transmission network which constitutes an infrastructure asset of special interest for the function of the entire city. The most crucial parts of a transmission line are the towers. Power transmission towers are usually tall steel lattice structures designed to support the conductors of a line. In most cases, towers are assembled in situ by elaborating steel angle profiles. In terms of function, one may distinguish two categories of towers: (1) Tangent or Support towers having vertical insulators and mainly carrying only gravity loads and (2) Angle/Dead-end towers, having two horizontal or inclined insulators per conductor, which are installed in specific points along a line in order to offer lateral resistance and/or allow changes in the direction of the line (Figure 38).

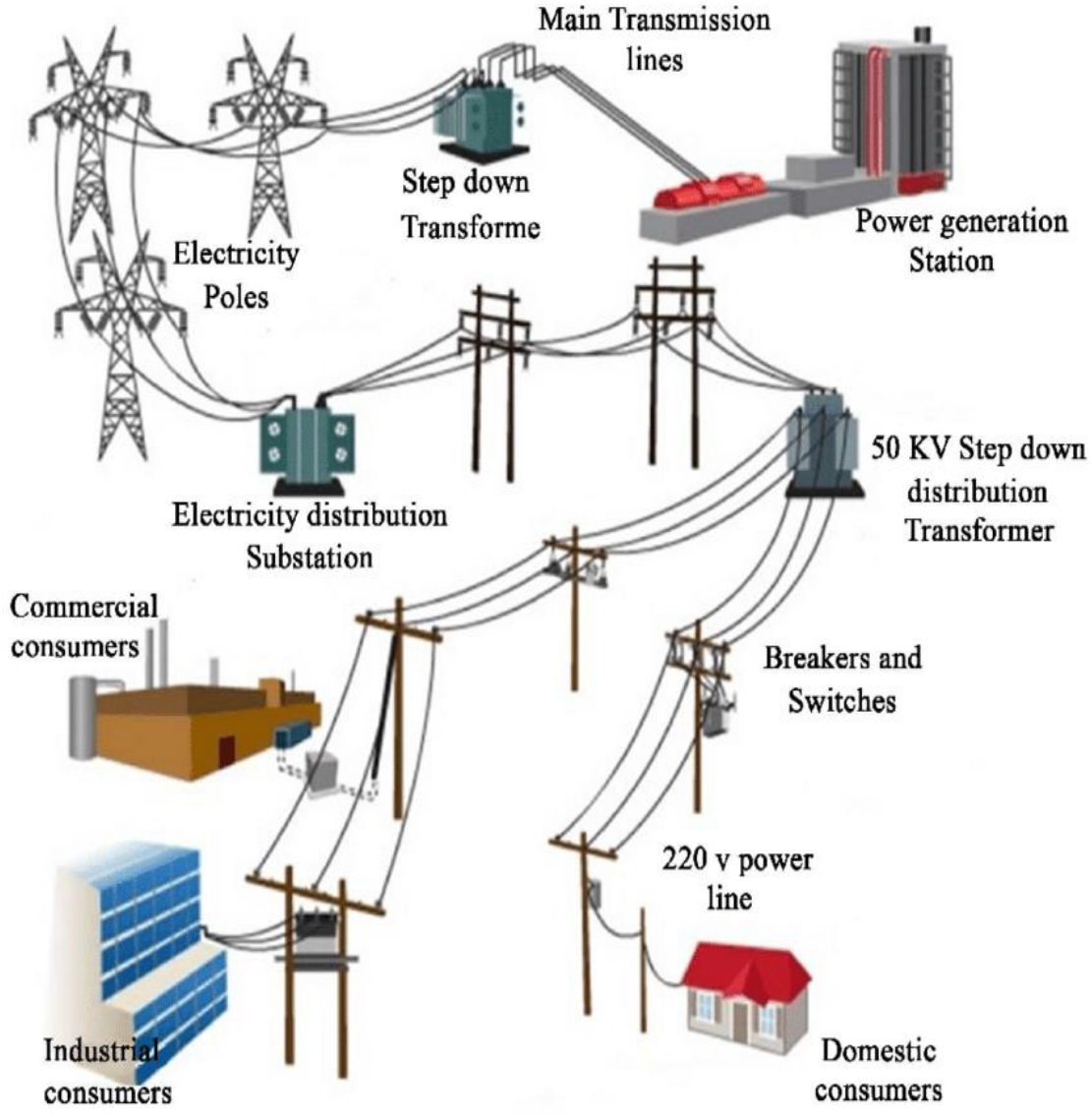

Figure 37: Schematic representation of the electrical power transmission system (https://afroasia.co.ke/power-transmission-distribution/).

The environmental action with the greatest loading effect on a transmission line is wind. Wind acts concurrently on the body of the tower (lattice structure) and on the conductors. Specifically, high wind speeds, usually in combination with low temperatures and the resulting ice accumulated on the exposed surface of the tower and the conductors, may increase the loads beyond the strength of the structure leading even to total collapse. This is because ice increases the loads on the structure in a twofold way, by raising the weight of the members and by increasing the wind force (due to the growth of the area of the exposed members and the conductors). Finally, it is noteworthy that in most cases the failure is not only observed in a single tower, but also in its adjacent ones (Figure 39) in a cascading effect, due to uneven distribution of tension forces in the conductor cables and the inability of support towers to carry along-line loads. This fact may lead to a major breakdown of a large part of the network with the corresponding impact to the provider and the consumers.

Figure 38: Typical types of power transmission tower configurations.

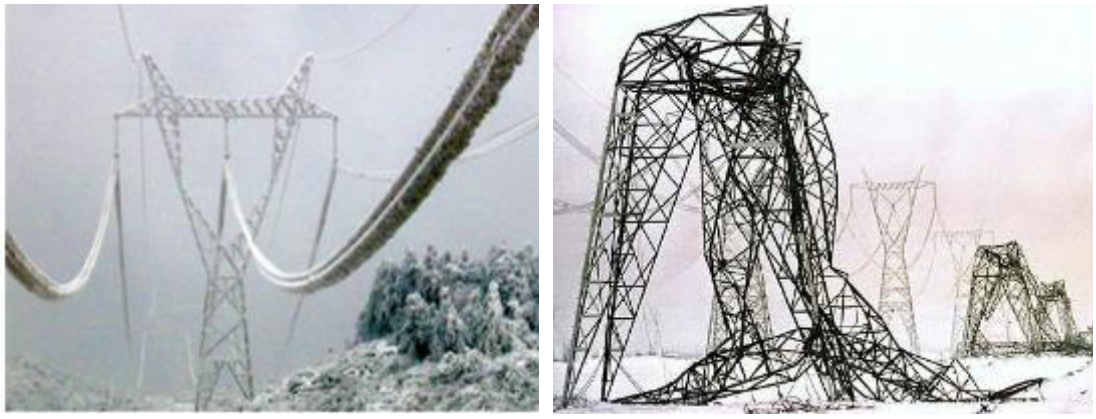

(a) (b)

Figure 39: (a) Ice on power transmission lines and (b) failure of power transmission line due to ice.

In most EU countries, an additional non-negligible factor is the age of the power transmission network, which was mainly built in the 50s and 60s. Nowadays, the largest part of the network (i.e. the transmission towers) exceeds the designed service life since it is in operation for more than fifty years. Thus, apart from the environmental factors mentioned above, age deterioration constitutes an additional source of risk that puts the operation of power networks into jeopardy.

The power transmission lines are classified in the Tier 3 category for HYPERION, thus only a few archetypes are modelled in detail to evaluate class-specific fragility and vulnerability functions. Specifically, the 3D model of an archetype power transmission tower is created via the OpenSees software (McKenna et al. 2000), as presented in Figure 40. It is assumed to be a support tower, thus the transverse and vertical loads due to conductors are simulated by applying the corresponding forces on the location of the insulators, while tension loads along the line direction are not accounted for. Horizontal springs are added to the model to simulate the earth-wire that is directly connected to the tower, thus transferring not only vertical but also lateral forces. The tower is modelled using both truss and beam elements with fibre sections having appropriately calibrated stress-strain relationships. Artificial wind time-histories are applied on the structure, while icing is also accounted for by repeating such analyses for a wide range of accumulated ice on the members, in order to estimate the structural response for a wide range of potential stressors. The IMs selected for the analysis are the 10-min mean wind speed and its direction as well as the equivalent ice thickness on the members, while the EDPs monitored are the deformations and the section moments and forces. More details can be found in Bilionis et al. 2020.

Measurements of the wind-stations are used for correlating wind and ice values with the expected failure patterns of the power transmission tower and prune down the large logic tree of potential consequences. The effect of CC is also considered to estimate potential damage realizations for the CC scenarios of WP3. Probabilistic age-dependent models are also developed based on the outputs of regular inspections and expert knowledge. The material properties of such models are modified to account for ageing, while the associated uncertainties are also incorporated.

The overhead distribution utility network constitutes a non-CH asset of significant importance for HYPERION, since its performance is related to the functionality of the entire city. The overhead distribution lines are primary supported by wood utility poles, which are less costly compared to the alternatives of e.g. concrete poles, but at the same time they can sustain considerable damage when subjected to high wind loads. They are exposed to the oxygen of the atmosphere and moisture, thus they are also susceptible to decay which significantly reduces their moment capacity. The utility network also comprises the conductors that are highly vulnerable to concurrent wind and ice loading. The accumulated ice around the steel conductors has a twofold effect: it increases their effective diameter thus higher lateral loads due to the wind are acting on the member, and also increases the weight of the conductor so larger gravity forces shall be carried by the network components. Damage on the utility network is mainly caused by failure of the supportive structures, i.e. the poles or the conductors (see for example Figure 41), and might result in power outage which significantly undermines the functionality of the city.

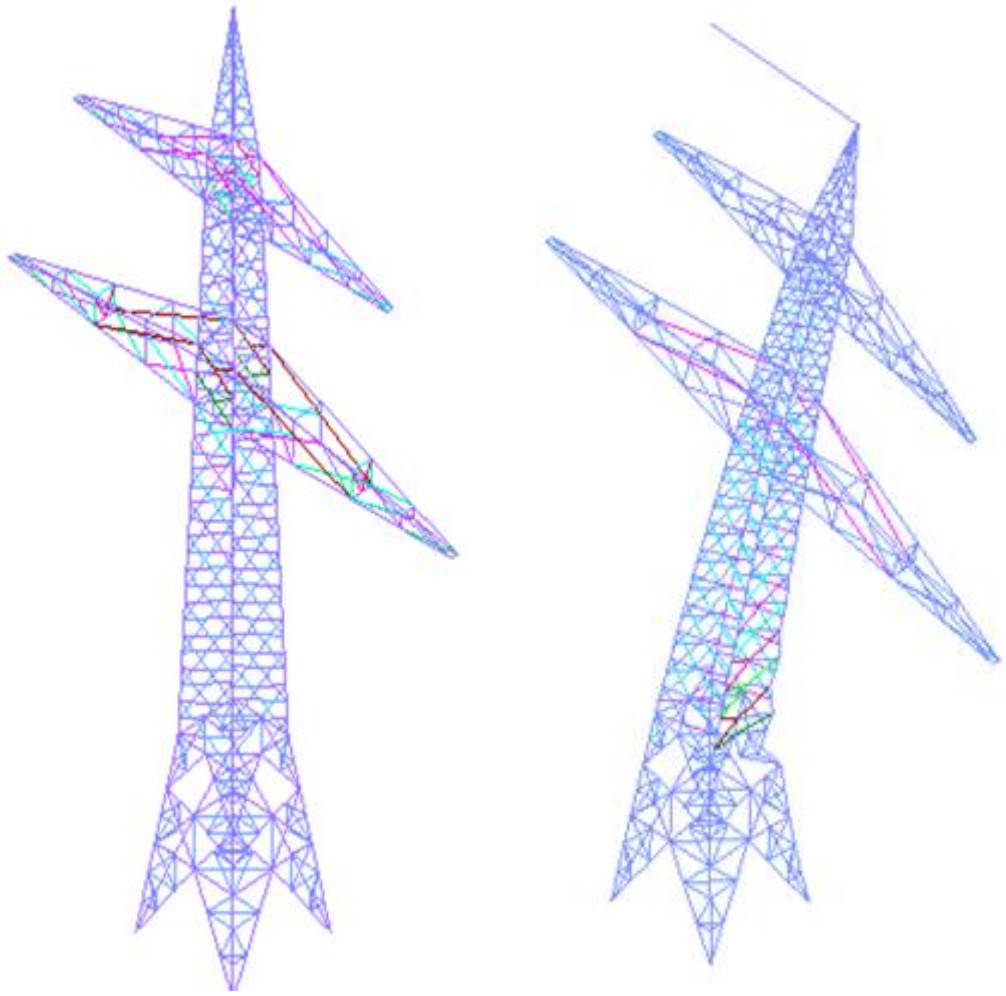

(a) (b)

Figure 40: (a) Nonlinear model of an index power transmission tower and (b) mechanism as revealed by pushover analysis (adopted from Bilionis et al. 2020).

The utility network of the city consists mainly of wood utility poles, as well as steel utility poles (Figure 42). Utility poles and conductors are classified in the Tier II category, thus only a limited number of archetypes are modelled analytically to estimate the class-specific fragility and vulnerability functions. The IMs considered in the analysis are the 10-min mean wind speed, u_{10}, its direction and the accumulated ice on the conductors, while the EDP that monitors their response is the drift of the pole and the moment at the ground level. The deterioration of the utility poles is accounted for by changing the initial MHVM to an already-run reduced-capacity MHVM and estimating again potential consequences. The reduced-capacity MHVM is created by employing deteriorated material properties on the wood and steel poles, based on inspection outcomes and expert opinion. Potential mitigation measures can be considered by improving the material properties and repeating the analysis. Wind measurements are used to correlate the recorded weather-related scenarios to potential damage on the utility network.

Figure 41: Failure of utility poles (Vivek et al. 2017).

Figure 42: Example of steel utility poles.

Electrical substations are critical facilities of the energy electric power distribution system, since they contain equipment such as relays, capacitor banks, batteries etc. that are needed to transform high voltage to low and vice versa, and also perform several other important functions. Most of the components and the main control building itself are vulnerable to the seismic action and it is very important that collapse or damage is prevented, since this might result in power outage with significant consequences for the entire city. Examples of damages on electric substations due to earthquakes are presented in Figure 43.

The electric substation is treated as a Tier 3 asset, thus class-specific fragility and vulnerability functions from literature are employed for risk assessment purposes. The IM selected for the analysis is the peak ground acceleration and the EDP for the

building is the drift. Multiple damage scenarios are generated based on the computed ground motion fields, while acceleration measurements are employed for pruning down the wide logic tree of potential ground motion fields to help estimate the consequences with more ease. An overview of critical parts of the power transmission network of Rhodes and Granada are shown in Figure 44 and Figure 45, respectively.

(a) main control room collapsed (b) damage on substations' components

Figure 43: Damages on electric substations and its components due to earthquakes (found in Liu et al. 2012).

Figure 44: Critical parts of the power transportation network of Rhodes island, Greece.

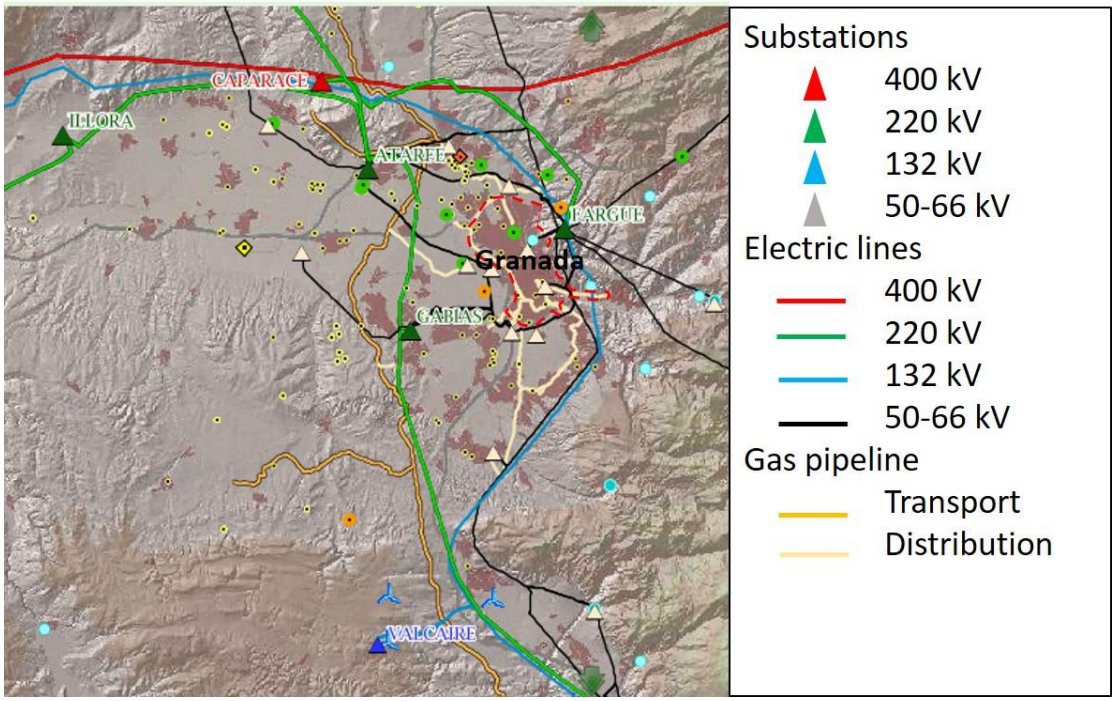

Figure 45: Critical parts of the power transportation network close to the Granada city (Spain) (https://www.agenciaandaluzadelaenergia.es)

3.2.5 Telecommunication antenna towers

Telecommunication towers are tall highly-optimized structures, similar to the power transmission towers, used by telecommunication network providers to support the microwave antennas. They are responsible for providing telecommunication connections and they are crucial to all incident management/response actions. In general, lack of telecommunication has been shown to be a significant impediment to timely action, severely affecting resilience. As in the case of the power transmission towers, the governing loading conditions are associated with low temperatures, ice and high winds. The effect of icing that is accumulated on the exposed members of the towers and on the surface of the antennas increases both the weight and the wind force on the structure (Figure 46).

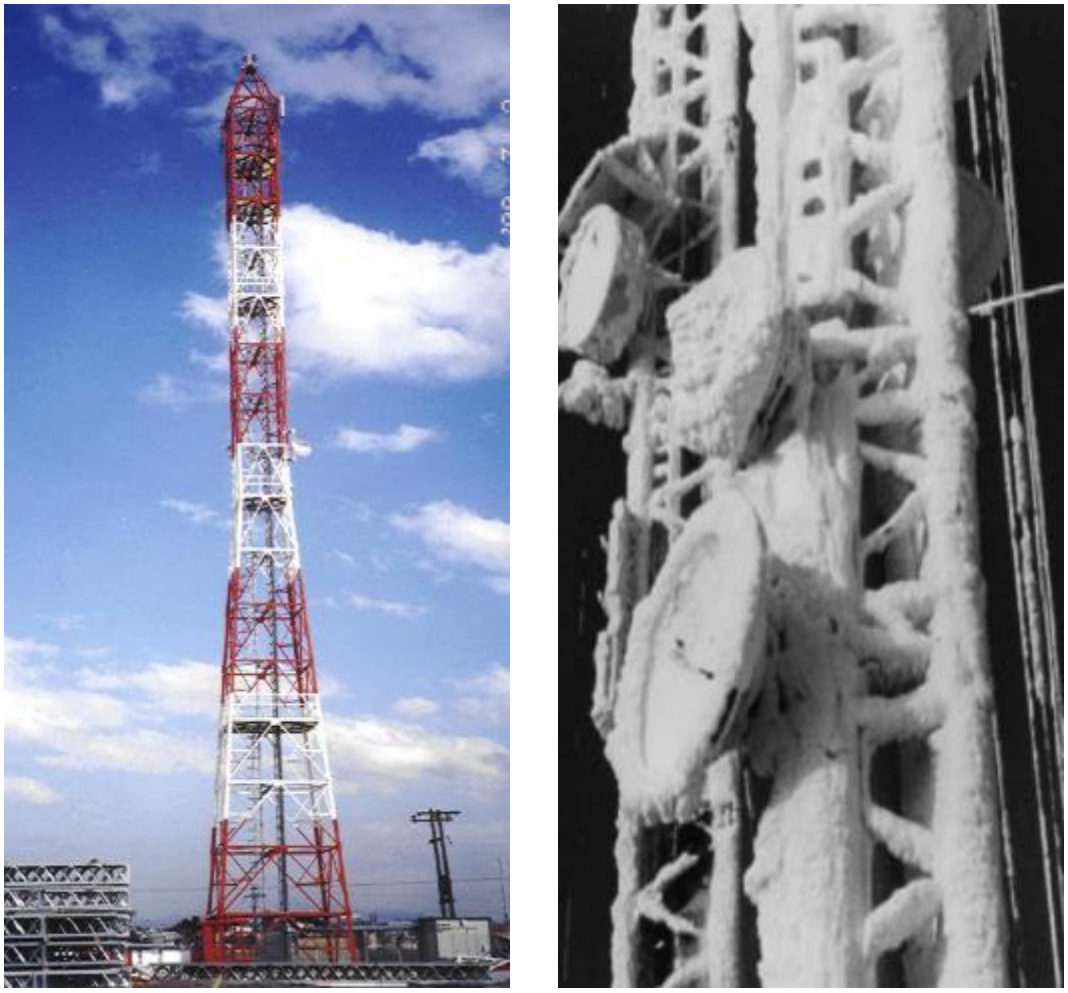

(a) (b)

Figure 46: (a) Typical telecommunication antenna tower and (b) ice on the tower (Sundin and Makkonen 1998).

The role of a telecommunication tower to carry the microwave antennas poses an additional challenge, especially when a need for upgrades in the telecommunication network occurs. In specific, network upgrades usually require the installation of larger and heavier antennas. In such a case, an existing tower may not be capable of carrying the increased loads. A common solution, other than taking down the existing tower and installing a new one, is tower strengthening. Tower strengthening is usually achieved by adding new members (e.g. angle beams) to the existing tower (Figure 47). In general, though, towers are often facing a reduction of structural reliability with each technology upgrade (2G→3G→4G→5G) this issue becoming critical with the scheduled deployment of 5G networks, as more and heavier antennas need to be deployed on the same towers to allow concurrent support of both older and newer generations of cellular telephony.

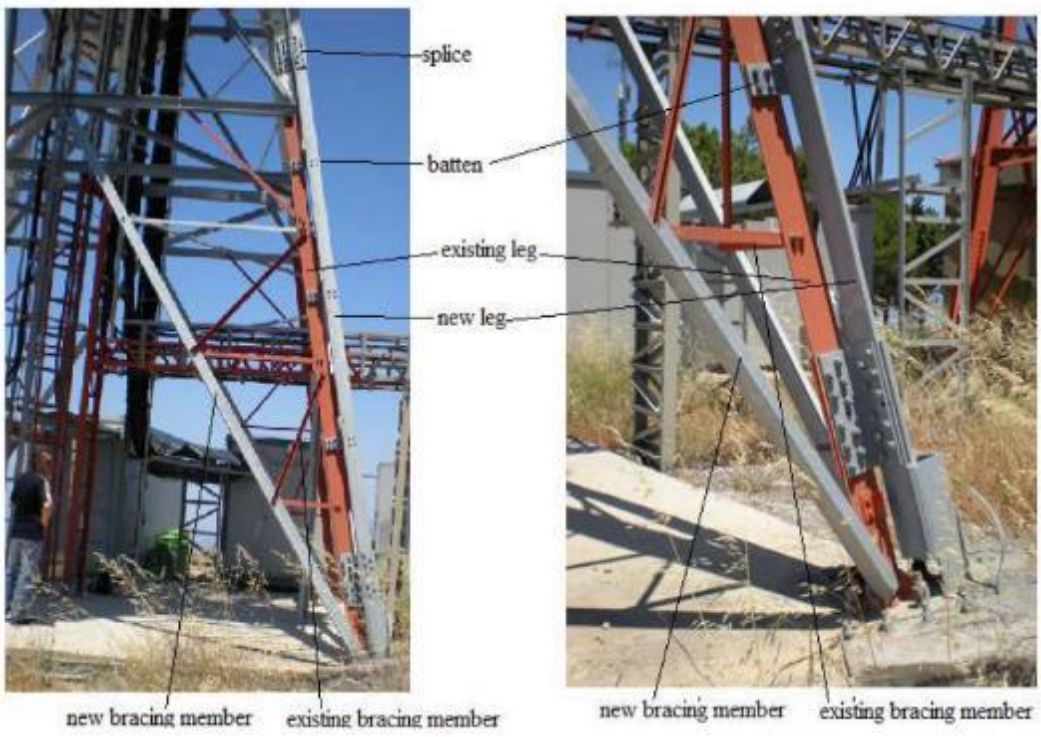

Figure 47: Strengthening of existing members.

Telecommunication towers are Tier 3 assets, thus only a limited number of archetypes are modelled analytically and used for fragility and vulnerability assessment using class-specific data. The model of the index telecommunication tower is shown in Figure 48 and is created via the OpenSees software (McKenna et al. 2000). It is composed of 932 members, both trusses and beams. The members are modelled as fibre sections beam-column or truss elements, sharing the same properties of the corresponding steel cross-sections of the structure. The IMs selected for the analyses are the 10-min mean wind speed, u_{10}, its direction and the accumulated ice on the members, while the EDP that monitors the structural response is the drift. Potential mitigation measures referring to the strengthening of the members, for instance using FRP members, can be accounted for by improving the material properties and repeating the analysis. Artificial wind time-histories are applied on the structure, while icing is also accounted for by repeating such analyses for a wide range of accumulated ice on the members, in order to estimate the structural response for a wide range of potential stressors. Wind measurements of the micro-weather stations are used to correlate the recorded weather-related scenarios to potential damage on the antennas.

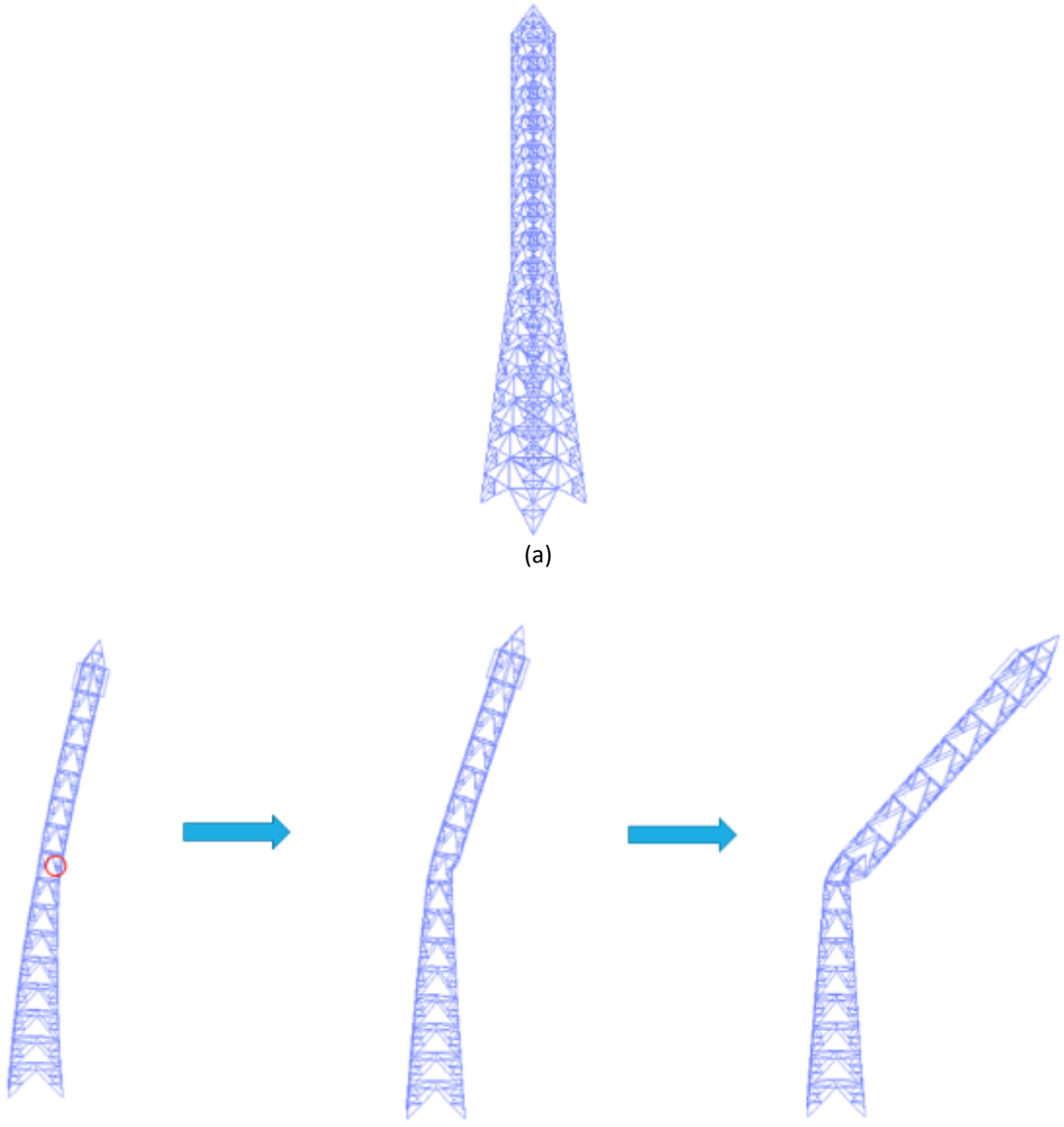

(a)

(b)

Figure 48: (a) 3D model of an index telecommunication tower and (b) failure mechanism as revealed by pushover analysis (adopted from Bilionis and Vamvatsikos 2019).

Figure 49 and Figure 50 present the location of telecommunication towers close to the city of Rhodes, and Venice.

Figure 49: Location of telecommunication antenna towers close to the city of Rhodes, Greece.

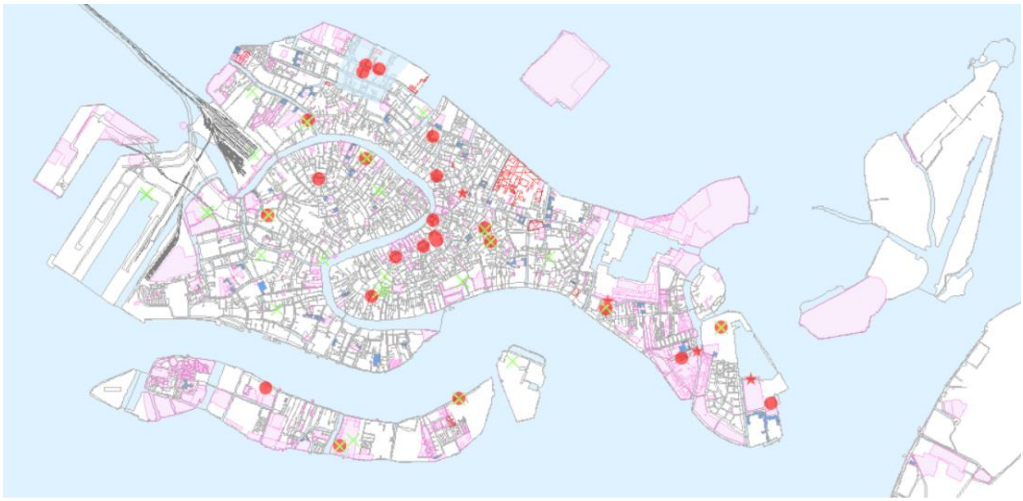

Figure 50: Location of telecommunication antenna towers in the city of Venice, Italy. (From the Municipality of Venice)

3.2.6 Analysis of assets

The assets that are considered for each test site are presented in detail in Deliverable D2.3 (Zeppos et al. 2019) and are listed in Table 15 through Table 18. For each asset, the IMs and EDPs are defined, while the consequences considered are monetary loss, downtime, business disruption etc. In Table 15 through Table 18, for each test site (city), the assets are classified based on the heritage rank (CH or non-CH), the tier (Tier 1, Tier 2 or Tier 3), the main construction material, the main hazard affecting their integrity/functionality, the considered intensity measure (IM) for the hazard and the engineering demand parameters (EDPs) for assessing the structural response.

Table 15: Granada assets

Asset	Heritage rank	Tier	Main material	Hazard	IM	EDP
San Jerónimo Monastery	CH	Tier 1	Stone masonry	Earthquake	PGA, $AvgS_a$	Interstory drift, internal forces and moments, deformations
The mill of the Marquis of Rivas	CH	Tier 2	Rammed earth, brick, stone	Earthquake	PGA, $AvgS_a$,	Interstory drift, internal forces and moments, deformations
Puerta Elvira	CH	Tier 2	Rammed earth, brick	Earthquake	PGA, $AvgS_a$	Deformations and section moment and forces
Fire house	non-CH	Tier 2	Steel	Earthquake, ice, ageing.	PGA, $AvgS_a$, long-term material properties degradation	Interstory drift, internal forces and moments, deformation, crack propagation.
Albayzín area	CH	Tier 3	Rammed earth, brick, stone	Earthquake	PGA, $AvgS_a$,	Drift moment forces, deformations
Realejo area	CH	Tier 3	Brick, stone, RC	Landslide, freeze-thaw cycles, earthquake	Mechanical properties of soil, long term soil deformation, extreme temperature, PGA, $AvgS_a$	Potential surface of the slope due to landslide, drift moment forces, deformations
Power transmission network	Non-CH	Tier 3	Steel	Wind, ice, ageing, earthquake	u_{10}, direction, long term material properties degradation, PGA, $AvgS_a$	Drift moment forces, crack propagation

Table 16: Rhodes assets

Asset	Heritage rank	Tier	Main Material	Hazard	IM	EDP
Saint Nikolas lighthouse and fort	CH	Tier 1	Stone	Earthquake, ageing	$AvgS_a$, time, moisture, temperature	Deformations, stress, strains
Nailac Pier	CH	Tier 1	Stone	Earthquake, ageing	$AvgS_a$, time, moisture, temperature	Deformations, stress, strains
The Roman bridge	CH	Tier 1	Stone	Earthquake, ageing	$AvgS_a$, time, moisture, temperature	Deformations, stress, strains
Grave enclosures in Rhodini	CH	Tier 1	Stone	Earthquake, ageing	$AvgS_a$, time, moisture, temperature	Deformations, stress, strains
Airport terminal	Non-CH	Tier 2	RC	Earthquake	$AvgS_a$	Interstory drift, internal forces and moments, deformations
Fire station	CH	Tier 3	Masonry	Earthquake	$AvgS_a$	Interstory drift, roof drift
Police station	CH	Tier 3	Masonry	Earthquake	$AvgS_a$	Interstory drift, roof drift
S. Aegean Regional building	CH	Tier 3	Masonry	Earthquake	$AvgS_a$	Interstory drift, roof drift
Municipality of Rhodes	CH	Tier 3	Masonry	Earthquake	$AvgS_a$	Interstory drift, roof drift
Central offices of Ephorate of the Dodecanese islands	CH	Tier 3	Masonry	Earthquake	$AvgS_a$	Interstory drift, roof drift
Power transmission network	Non-CH	Tier 3	Steel	Wind, ageing	u_{10}, direction	Drift, moment, forces
Telecommunication antenna towers	Non-CH	Tier 3	Steel	Wind, ageing	u_{10}, direction	Drift, moment, forces
Military Headquarters	Non-CH	Tier 3	RC	Earthquake	$AvgS_a$	Interstory drift, roof drift

Public services building	Non-CH	Tier 3	RC	Earthquake	$AvgS_a$	Interstory drift, roof drift
Regional Hospital	Non-CH	Tier 3	RC	Earthquake	$AvgS_a$	Interstory drift, roof drift
"Kremasti" bridge	Non-CH	Tier 3	RC	Earthquake, flooding	$AvgS_a$, water height	Drift
Water and sewage network	Non-CH	Tier 3	--	Earthquake	PGV	Stress, strain
Other buildings	CH and non-CH	Tier 3	RC, masonry	Earthquake, flooding	$AvgS_a$, water height	Drift, flooded area

Table 17: Tønsberg assets

Asset	**Heritage rank**	**Tier**	**Main material**	**Hazard**	**IM**	**EDP**
Western Tower	CH	Tier 1	Stone	Biodegradation	Mould or lichen growth rate	Erosion rate
The Heierstad Loft	CH	Tier 1	Timber	Extreme wind, foundation settlement	Speed and direction of wind, possible settlement	Interstory drift, internal forces
The Fadum Store house	CH	Tier 1	Timber	Extreme wind, foundation settlement	Speed and direction of wind, possible settlement	Interstory drift, internal forces
Bentegården	CH	Tier 1	Timber	Extreme wind, flood	Speed and direction of wind	Interstory drift, internal forces
Slottsfjell Tower	CH	Tier 2	Stone masonry	Extreme wind, creep	Speed and direction of wind, long term material properties	Interstory drift, internal forces, crack propagation

City of Tønsberg	Non-CH	Tier 3		Fire, extreme wind, quick clay landslide	Fire emergency system availability, speed and direction of wind, mechanical properties of soil, long term soil deformation	Fire propagation rate, loss due to wind, potential surface of the slope due to landslide

Table 18: Venice assets

Asset	Heritage rank	Tier	Main material	Hazard	IM	EDP
Torre dell'Orologio	CH	Tier 1	Stones (Istrian stone and white marbles)/bricks	Tidal fluctuation; strong wind and storms; freeze/thaw cycles.	Highest and lowest astronomical tide; wind speed (u_{10}) and direction; precipitation intensity; extreme temperatures.	Hydrostatic pressures; surface recession; erosion of foundations; drift moment forces; cracks propagation.
Buildings from *Piazzale Roma* to the Accademia bridge	CH	Tier 2	Stones/bricks	Tidal fluctuation; strong wind and storms; freeze/thaw cycles.	Highest and lowest astronomical tide; wind speed (u_{10}) and direction; precipitation intensity; extreme temperatures.	Hydrostatic pressures; surface recession; erosion of foundations; drift moment forces; cracks propagation.
Rialto bridge	CH	Tier 2	Istrian stone, *Pietra di Muggia*	Tidal fluctuation; freeze/thaw cycles; daily water transport.	Highest and lowest astronomical tide; extreme temperatures; water displacement and wave-induced motion; pollution due to exhaust	Hydrostatic pressures; erosion of foundations; cracks propagation; decay products.

					gases from ships.	
The Mercerie	CH	Tier 2	Stone/bricks	Tidal fluctuation; freeze/thaw cycles.	Highest and lowest astronomical tide; extreme temperatures.	Hydrostatic pressures; erosion of foundations; cracks propagation.
The Giudecca canal	CH	Tier 2	Stones/bricks	Tidal fluctuation; transit of large cruise ships.	Highest and lowest astronomical tide; water displacement and wave-induced motion; pollution due to exhaust gases.	Hydrostatic pressures; erosion of foundations; drift moment forces; cracks propagation; corrosion; decay products.
Ca' Pesaro Palace	CH	Tier 2	Istrian stone/bricks	Tidal fluctuation; strong wind and storms; freeze/thaw cycles.	Highest and lowest astronomical tide; wind speed (u_{10}) and direction; precipitation intensity; extreme temperatures.	Hydrostatic pressures; surface recession; erosion of foundations; drift moment forces; cracks propagation.
Civil Hospital	CH	Tier 2	Stones (marbles)/bricks	Tidal fluctuation; strong wind and storms; freeze/thaw cycles.	Highest and lowest astronomical tide; wind speed (u_{10}) and direction; precipitation intensity; extreme temperatures.	Hydrostatic pressures; surface recession; erosion of foundations; drift moment forces; cracks propagation.
Ponte della Libertá	Non-CH	Tier 2	Bricks/stones/concrete	Tidal fluctuation; strong wind; freeze/thaw cycles; daily traffic (road transport and railway).	Highest and lowest astronomical tide; wind speed (u_{10}) and direction; extreme temperatures; pollution due	Hydrostatic pressures; erosion of foundations; drift moment forces; cracks propagation;

					to exhaust gases	decay products.
The Marciana area	CH	Tier 3	Stones/bricks	Tidal fluctuation; strong wind and storms; freeze/thaw cycles.	Highest and lowest astronomical tide; wind speed (u_{10}) and direction; precipitation intensity; extreme temperatures.	Hydrostatic pressures; surface recession; erosion of foundations; drift moment forces; cracks propagation, corrosion.
Airport	Non-CH	Tier 3	RC/bricks/steel/glass	Tidal fluctuation; strong wind and storms; freeze/thaw cycles; air traffic.	Highest and lowest astronomical tide; wind speed (u_{10}) and direction; precipitation intensity; extreme temperatures; pollution due to exhaust gases	Hydrostatic pressures; erosion of foundations; decay products.
Port	Non-CH	Tier 3	RC	Tidal fluctuation, water traffic	Highest and lowest astronomical tide; pollution due to exhaust gases.	Corrosion; decay products.
Industrial site of Porto Marghera	Non-CH	Tier 3	RC	Tidal fluctuation; strong wind and storms; freeze/thaw cycles; strong air and soil pollution due to transports and industrial installations	Highest and lowest astronomical tide; wind speed (u_{10}) and direction; precipitation intensity; extreme temperatures; pollution due to exhaust gases.	Hydrostatic pressures; erosion of foundations; drift moment forces; crack propagation, corrosion; decay products.
Telecommunication antenna towers	Non-CH	Tier 3	steel	Tidal fluctuation, wind.	Highest and lowest astronomical tide; u_{10}, direction.	Erosion of foundations; corrosion; drift moment forces.

4 Description of MHVM structure

The Multi-Hazard Vulnerability Module consists of two files for each asset or class: the scenario MSA file, named "*name.*msa.mat/xml", and the metadata file, named "*name.*mtdata.mat/xml", where *name* is the name of the asset. Data of both files are combined for the pre-event vulnerability assessment of each individual asset, to generate multiple damage/consequences scenarios. The individual asset's scenarios are later combined with the IM fields to form multiple scenarios that may happen in the entire test site in the pre-event operation phase of HYPERION, as schematically shown in Figure 51. In this phase, risk assessment of the entire test site is performed, and all "possible" scenarios are calculated and their consequences in terms of damage and recovery are assessed, by combining the hazard results of all individual assets. This detailed picture of "all" events that can happen, together with the damage and loss prediction, lead to a growing large tree of potential events, which can later be pruned in the trans-event operation phase, to help HYPERION achieve its goal of sensor-driven near-real-time assessment. In the trans-event phase, where the event has just happened (or is presently unfolding), the limited information that is available, especially from the sensors, is used to prune the set of potential scenarios into a more manageable size of most probable outcomes, that can guide the operators better than a full-fledged assessment of what could have happened (without any sensor information).

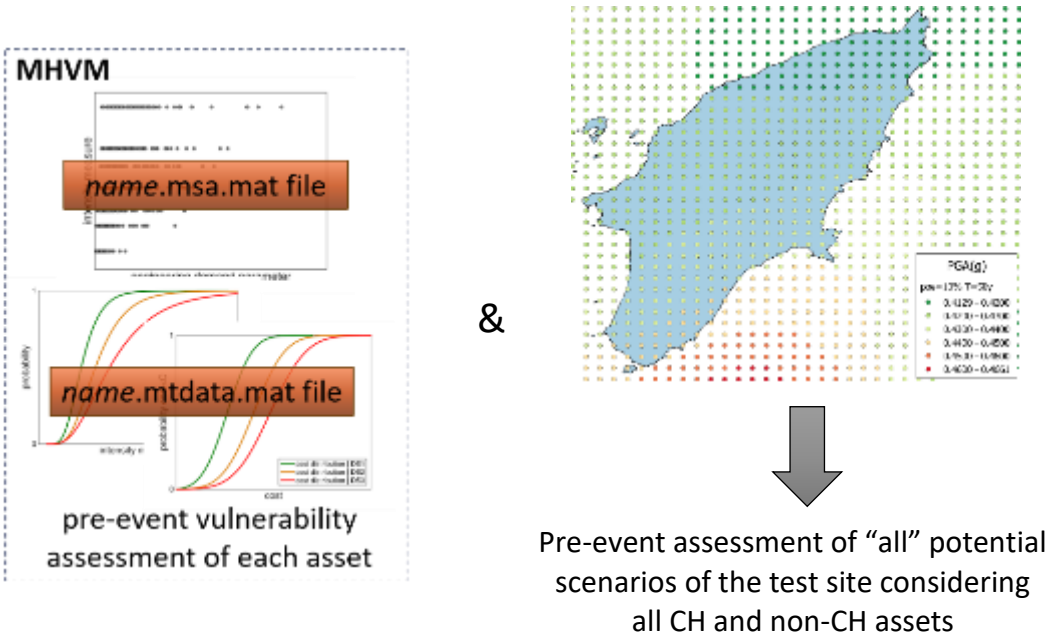

Figure 51: Pre-event assessment of "all" potential scenarios of the Rhodes' test site by combining the MHVM with the IM fields.

4.1 Metadata file

The asset-specific metadata file contains information on the fragility curves and the consequence functions (e.g. repair cost, downtime etc.) associated with each damage state. The fragility functions of Tier 3 and any Tier 1, Tier 2 assets that receive a system-only treatment are probability-valued functions of the IM of choice (e.g. peak ground acceleration for the seismic hazard or wind speed for the wind hazard), that can define the damage state of the entire structure but not of its individual components. For the assets that are treated via a component-based approach, component-specific fragility and consequence functions conditioned on the component's EDP are defined and used for risk estimation. The general format of the metadata file is the same for assets receiving a component-based or a system-only treatment, with only some details differing among these two cases. The metadata files in both cases are named by the asset's name, followed by the extension ".mtdata.mat/xml", e.g. "StJerMon.mtdata.m/xml" for the Saint Jeronimo Monastery in Granada, Spain. A metadata file in xml format is also adopted for the assets, since this format is better suited for risk assessment of the entire network via the Python® software, while the .mat file is used for generating individual asset scenarios through the MATLAB® software, for the assets that receive a component-based treatment. For this reason, the metadata of each asset can be stored in either .mat or .xml format, and available software interfaces are used to convert one format to the other.

4.1.1 Metadata file Tier 1 and Tier 2 assets that receive a component-based treatment

The mtdata.mat file

A typical mtdata.mat file for Tier 1 and Tier 2 assets treated via a component-based procedure is created using MATLAB® software (www.mathworks.com), as shown in Figure 52. The fields of this file are presented in detail in this section.

Figure 52: Typical metadata file for assets treated via a component-based approach.

Figure with component serial numbering

For this type of assets, a component-based procedure is followed, thus a figure with the serial numbering of all critical components is needed. A bridge (for example the bridge connecting Venice historical centre to the mainland) is presented for illustrative purposes in Figure 53, where the bearings and the piers are the critical assets numbered. This figure is stored in the ".SerialNumberingFig" field of the mtdata.mat file. Note that the component numbering should be consistent with the multi-stripe analysis results. This means that the results of bearing 1 are found in the first entry of the EDP value associated with the bearings, the results of bearing 2 in the second entry etc.

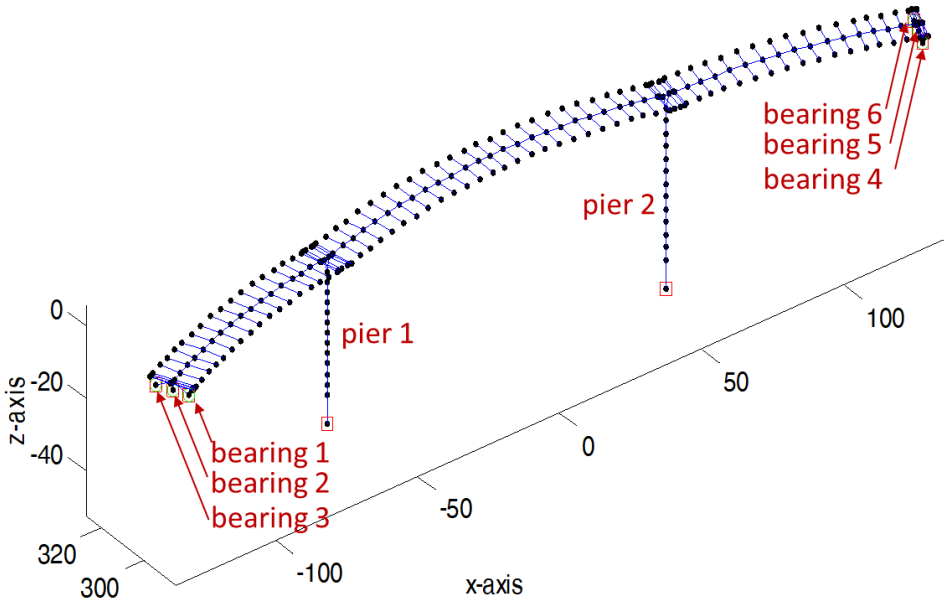

Figure 53: Typical figure of serial numbering and description of components for a bridge (stored in the .SerialNumberingFig field of the *AssetName*.mtdata.mat file).

Component's data

Data for each component are stored in the ".ComponentsData" field of the mtdata.mat file. In this field, generic categories of components are defined along with their associated engineering demand parameters (EDPs), fragility and consequence functions. Note that the engineering demand parameter should be the same as the corresponding EDPlabel of the MSA results. An example of ".ComponentsData" is presented in Figure 54, where the generic categories of Bearing.001, Bearing.002 and Pier.001 are defined, along with the EDP that governs their response (dummy data) and the associated Damage States, *DS*, fragility curves, *fragpar*, cost, *costpar*, traffic reduction, *trafredpar*, and downtime, *downpar* functions. In Figure 55, four sequential damage states are defined for the component along with the fragility data. Each fragility curve is assumed to follow the lognormal distribution (2nd column) with the parameters of the 3rd column of each damage state entry.

Fields	name	EDP	DS	fragpar	costpar	trafredpar	downtimepar
1	'Bearing.001'	'maxbdr_srss'	1x4 cell	4x3 cell	4x2 cell	4x2 cell	4x2 cell
2	'Bearing.002'	'maxbdrx'	1x4 cell	4x3 cell	4x2 cell	4x2 cell	4x2 cell
5	'Pier.001'	'maxidr_srss'	1x4 cell	4x3 cell	4x2 cell	4x2 cell	4x2 cell

Figure 54: Example of definition of component's data for a bridge (*AssetName*.mtdata.mat, .ComponentsData field).

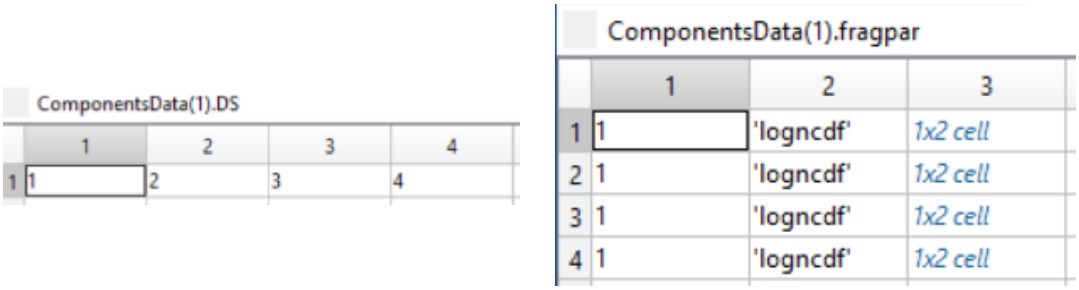

(a) (b)

Figure 55: Example of (a) damage states and (b) fragility curve definition for a component (*AssetName*.mtdata.mat, .ComponentsData.DS and .ComponentsData.fragpar field).

Units

The units of each consequence function are defined in the ".Units" field along with a short description of each consequence function. An example of the units entry is shown in Figure 56.

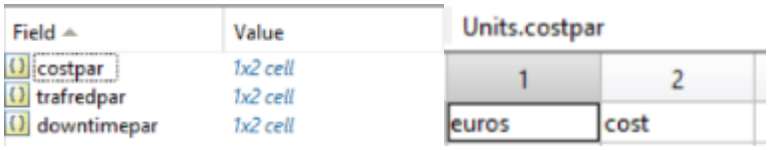

Figure 56: Example of consequence functions units definition (*AssetName*.mtdata.mat, .Units field).

Asset's components

The ".Components" field of the mtdata.mat file contains information on the components of the specific asset that are considered for risk estimation. It is a cell array in MATLAB whose *i* = 1….*N* (or {1,N} in MATLAB terminology) entries correspond to the components with serial number *i* = 1….*N*. Two entries are expected for each component, namely the name of the category of the component that must be consistent with naming of fragility and consequence functions and the number of such components. For example, the definition of ".Components" field of bridge can be seen in Figure 57, assuming that all bearings are of the same generic bearing type of Bearing.001 and both piers of type Pier.001.

```
% define the components of the asset
metad.Components{1}={'Bearing.001',1,'Pier.001',1};
metad.Components{2}={'Bearing.001',1,'Pier.001',1};
metad.Components{3}={'Bearing.001',1};
metad.Components{4}={'Bearing.001',1};
metad.Components{5}={'Bearing.001',1};
metad.Components{6}={'Bearing.001',1};
```

Figure 57: Example of component definition for a bridge (*AssetName*.mtdata.mat, .Components field).

Asset's data

In the ".AssetsData" field of the mtdata.mat file, some generic functions of the asset are defined, such as generic collapse fragilities and consequence functions that are used to determine if the asset has collapsed (e.g. in case of deck unseating of a bridge). Moreover, demolition and consequences for replacing the asset are also defined.

The mtdata.xml file

The xml file with the metadata for a Tier I or Tier II asset that is treated via a component-based approach is presented in Figure 58, where dummy values are used for the fragility and consequence functions. The same information is stored in both the .mat and .xml files of an asset; only the format differs. In the "ComponentsFigureFile" entry the name of the figure with the asset's components is defined, the "Components" entry includes all individual components along with their ID, taxonomy, number of such components per asset, and the EDP label, as well as its index where the MSA results for the specific component can be found. The taxonomy is used to link each individual component with the fragility and consequence functions, that are defined in the "FragilityFunctions" and "ConsFunctions" entries, respectively. The distribution they follow is set in the corresponding "dist" entries, along with the number of damage states and the parameters of such distributions. The type of the consequence functions is also defined in the "cons_id" entry and its units in "units", for instance "cost" and "euros" can be used to calculate economic consequences in euros. Finally, a description of the asset follows as well as potential references.

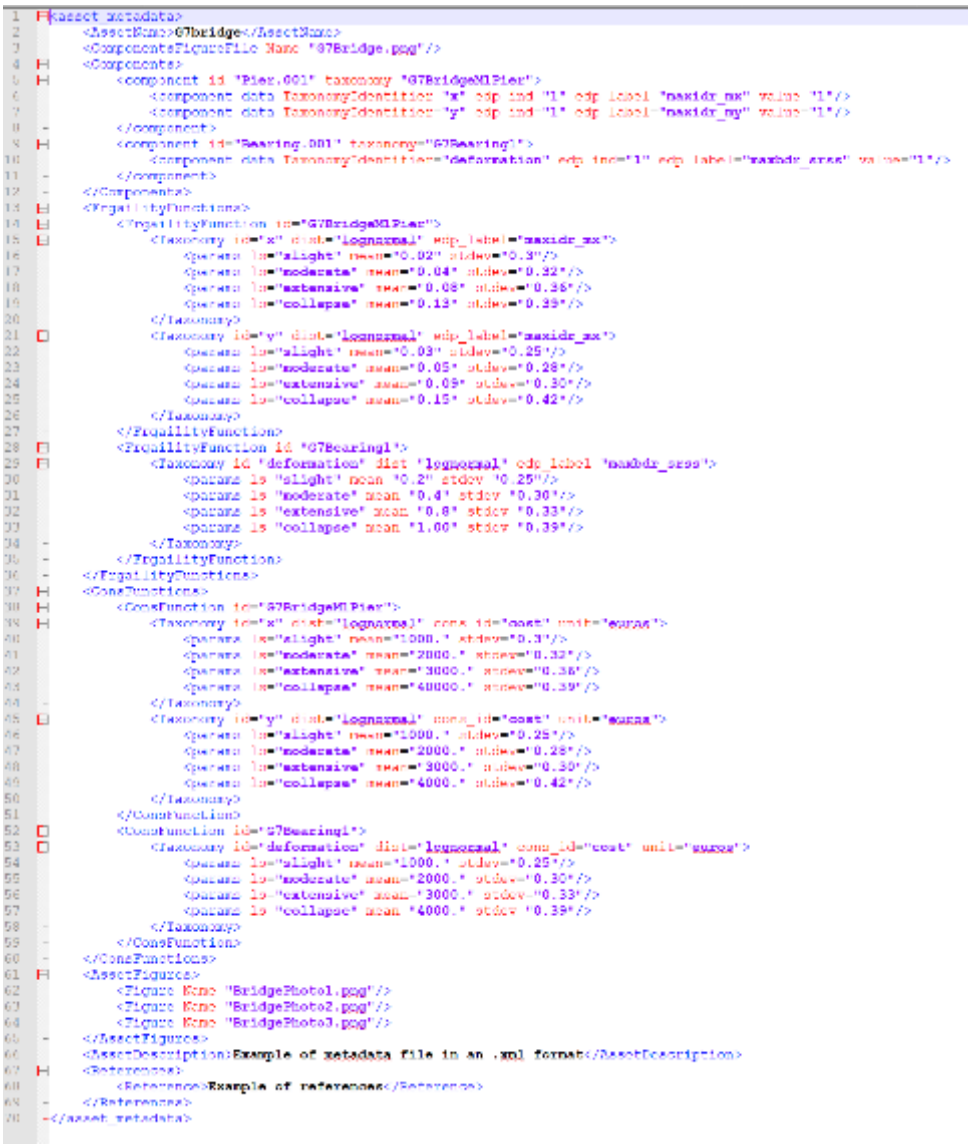

Figure 58: Example of the mtdata.xml file for a bridge (*AssetName*.mtdata.mat, .Components field).

4.1.2 Metadata file Tier 3 assets that receive a system-only treatment

The mtdata.mat file

A typical metadata file for Tier 3 assets treated via system-only approach, i.e. for asset with generic fragility and consequence functions, is presented in Figure 59. The fields of this file are “AssetsData” and “Units”, where the name of the IM and the corresponding fragility and consequence functions are defined and the units with a short description of the consequence functions are set, as shown in Figure 60 and Figure 61, respectively.

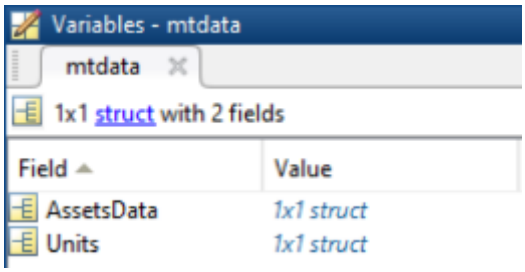

Figure 59: Typical metadata file for Tier 3 assets treated via a system-only approach.

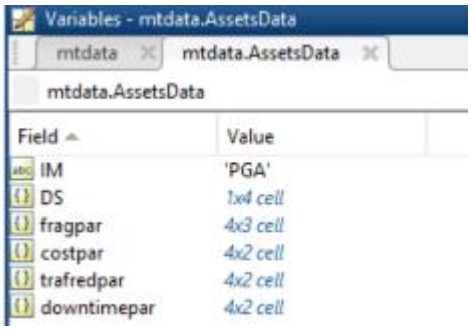

Figure 60: Example of IM, damage states and fragility/consequence function definition (*AssetName*.mtdata.mat, .AssetsData field).

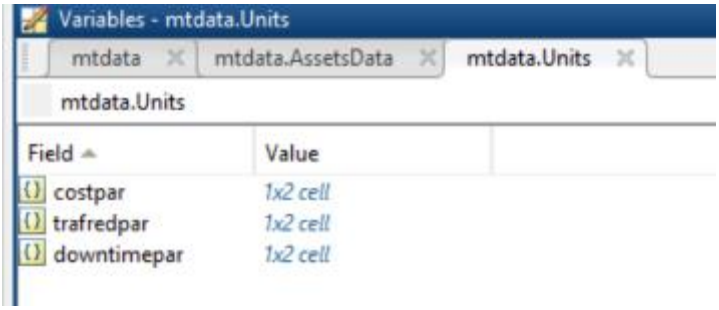

Figure 61: Example of units definition (*AssetName*.mtdata.mat, .Units field).

The mtdata.xml file

An example of the .xml file containing an asset's metadata is presented in Figure 62. For each asset, generic fragility and consequence functions are defined and stored in the "FrgailityFunctions" and "ConsFunctions" entries, respectively. The IM that controls the response of the asset is defined in the "IM" instance of the fragility functions, along with the corresponding damage states and the associated consequences.

Figure 62: Example of a Tier 3 asset's metadata file in xml format.

4.2 Scenario Multi-Stripe Analysis file

The scenario MSA file contains the multi-stripe analysis results following the format defined in this section.

4.2.1 Intensity measure levels

To enable the assessment for each of the CH and non-CH assets, the following IMs are identified per stressor:

- earthquake: an array of *IM* levels characterised by the first mode spectral acceleration, $S_a(T_1,5\%)$, or the average spectral acceleration, $AvgS_a$. This is going to be indicated via the 'im_range' variable (see also Figure 63).
- wind: two vectors should be provided in that instance, namely the wind speed (e.g. in m/s) and the direction (e.g. in degrees). The grid should be automatically generated in Matlab via the 'meshgird' function.
- temperature: typically in ^oC
- precipitation: typically in mm of water over a given time period
- ice thickness: this is the thickness of ice on steel members, estimated from precipitation and temperature data as a cascading IM

4.2.2 EDP response levels per each numbered component and IM level

Each scenario MSA file contains a number of variables that can be exploited during post-processing (Figure 63). A short description for each of these variables is summarised below:

- *EDPlabel*: strings containing the variable names for each of the *EDPs* recorded
- *EDPsublab*: strings containing a short description for each of the *EDP* variables
- *EDPval*: recorded *EDP* values. Output format as follows:

size(*EDPval*) = 1 x length(*EDPlabel*)

size(*EDPval*{1}) = 1 x length(*IM* levels)

- for global (i.e. asset-level) measurements,

length(*EDPval*{1,1}{1,1}) = 1

- for local (i.e. spoke (or component)-level) measurements,

length(*EDPval*{2}{1,1}) = #components

- *im_range*: range of *IM* values (i.e. stripe *IM* levels)
- *runs*: number of analysis runs per *IM* level
- *T_periods*: The first *N* vibration periods of the structure (where *N* is determined by the user in the structural analysis software)
- *thfilename*: loading history file names

The following variables are also stored for seismic response analysis:

- *record_pga*: each record's (and component's) *PGA*
- *record_psa*: each record's (and each component's) pseudo-$S_a(T_{i,x}\%)$ values for each of the periods found in *T_periods*
- *record_sa*: each record's (and each component's) $S_a(T_{i,x}\%)$ values for each of the periods found in *T_periods*

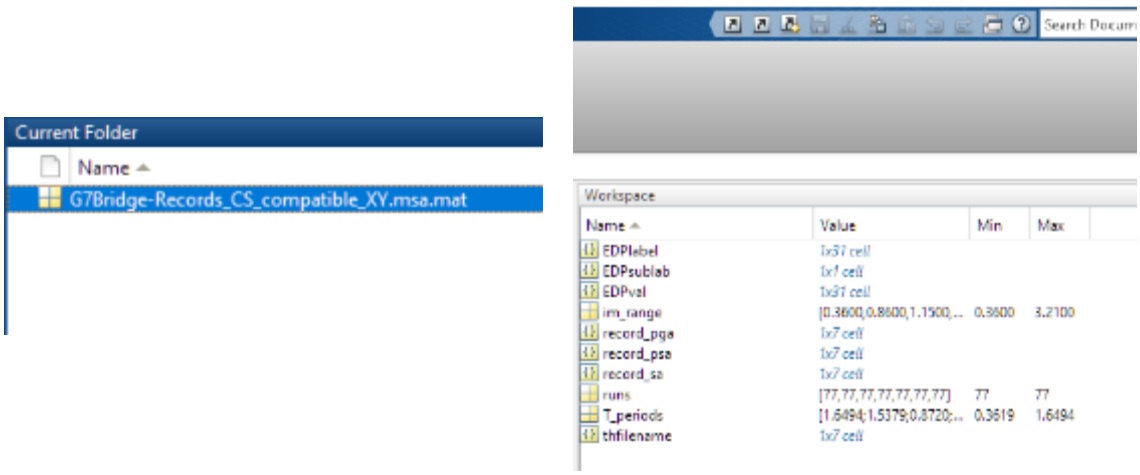

(a) (b)

Figure 63: (a) Scenario MSA file example and (b) variables contained in a scenario MSA file.

5 References

Avdelidis N.P., Moropoulou A., Theoulakis P. (2013) Detection of water deposits and movement in porous materials by infrared imaging, Infrared Physics & Technology 44 (2003) 183–190. doi:10.1016/S1350-4495(02)00212-8

Applied Technology Council (ATC). (2009). Development of next generation performance-based seismic design procedures for new and existing buildings.

Baker, J. W. (2015). Efficient analytical fragility function fitting using dynamic structural analysis. Earthquake Spectra, 31(1), 579–599. DOI: 10.1193/021113EQS025M

Bilionis, D. V. & Vamvatsikos, D. (2019). Wind performance assessment of telecommunication towers: a case study in Greece. 7th ECCOMAS Thematic Conference on Computational Methods in Structural Dynamics and Earthquake Engineering, COMPDYN 2019.

Bilionis, D. V., Bezas, M. Z., Tibolt, M., Vamvatsikos, D., & Vayas, I. (2020). Performance-based assessment of a steel lattice power-transmission tower: A case study in Germany. 9th European Conference on Steel and Composite Structures, EUROSTEEL 2020.

Cornell, C. A. & Krawinkler, H. (2000). Progress and challenges in seismic performance assessment. PEER Center News 2000, 3(2), 1–4.

Cornell, C. A. (1968). Engineering seismic risk analysis. Bulletin of the Seismological Society of America, 58(5), 1583-1606.

Cornell, C. A., & Jalayer, F. (2002). Factored nonlinear displacement demand estimation methods for probability-based safety assessment. In Annual Meeting Research Digest No. 2002-7, A publication of the Pacific Earthquake Engineering Research Center: Berkeley, CA, 2002, pp. 1–4.

D'Ayala, D., Meslem, A., Vamvastikos, D., Porter, K., Rossetto, T., Crowley, H., & Silva, V. (2015). Guidelines for analytical vulnerability assessment of low/mid-rise Buildings, Vulnerability Global Component project. DOI: 10.13117/GEM.VULN-MOD.TR2014.12

Jalayer, F. & Cornell, C. A. (2009). Alternative non-linear demand estimation methods for probability-based seismic assessments. Earthquake Engineering & Structural Dynamics, 38(8), 951–972. DOI: 10.1002/eqe.876

Jalayer, F. (2003). Direct Probabilistic Seismic Analysis: Implementing non-linear dynamic assessments. Ph.D. dissertation, Dept. of Civil and Environmental Engineering, Stanford Univ., Stanford, CA.

Jalón, M., Chiachío J., Gil, L.M., & Montes, E. (2020) Probabilistic identification of surface recession patterns in heritage buildings based on digital photogrammetry. Submitted to Journal of Building Engineering.

Krommyda, M. & the HYPERION Consortium (2020). Architecture specification. Deliverable D2.3 URL https://www.hyperion-project.eu/deliverables/

Lin, T., Haselton, C. B., & Baker, J. W. (2013). Conditional spectrum-based ground motion selection. Part I: Hazard consistency for risk-based assessments. Earthquake Engineering & Structural Dynamics, 42(12), 1847–1865. DOI: 10.1002/eqe.2301

Liu, R., Zhang, M., & Wu, Y. (2012). Vulnerability study of electric power grid in

different intensity area in Wenchuan Earthquake. In 15th World Conference of Earthquake Engineering (WCEE), Lisboa, Portugal.

Luco, N. & Cornell C. A. (2007). Structure-Specific scalar intensity measures for near-source and ordinary earthquake ground motions. Earthquake Spectra, 23(2), 357–392. DOI: 10.1193/1.2723158

Luque A., Leiss B., Alvarez-Lloret P., Cultrone G., Siegesmund S., Sebastián E., Cardell C. (2011) Potential thermal expansion of calcitic and dolomitic marbles from Andalusia (Spain), Journal of Applied Crystallography 44(6)

Germinario L., Siegesmund S., Maritan L. Mazzoli C. (2017) Petrophysical and mechanical properties of Euganean trachyte and implications for dimension stone decay and durability performance, Environmental Earth Sciences volume 76, Article number: 739. doi.org/10.1007/s12665-017-7034-6

Mackie, K. & Stojadinovic, B. (2001). Probabilistic seismic demand model for California highway bridges. Journal of Bridge Engineering, 6(6), 468–481. DOI: 10.1061/(ASCE)1084-0702(2001)6:6(468)

McKenna, F., Fenves, G. L, and Scott, M. H. (2000) Open System for Earthquake Engineering Simulation. University of California, Berkeley, http://opensees.berkeley.edu.

Miano, A., Jalayer, F., De Risi, R., Prota, A., & Manfredi, G. (2016). Model updating and seismic loss assessment for a portfolio of bridges. Bulletin of Earthquake Engineering, 14(3), 699–719. DOI: 10.1007/s10518-015-9850-y

Molina E., Cultrone G., Sebastián E., Alonso F.J. (2013) Evaluation of stone durability using a combination of ultrasound, mechanical and accelerated aging tests, Journal of Geophysics and Engineering, Volume 10, Number 3, doi.org/10.1088/1742-2132/10/3/035003

Navarro R., Cruz A.S., Arriaga L., Baltuille J. M. (2013) White Macael marble: a key element in the architectonic heritage of Andalusia for over 25 centuries, Conference: EGU General Assembly 2013At: Vienna Volume: Geophysical Research Abstracts Vol. 15, EGU2013-4252-1

Padgett, J. E., & DesRoches, R. (2008). Methodology for the development of analytical fragility curves for retrofitted bridges. Earthquake Engineering & Structural Dynamics, 37(8), 1157–1174. DOI: 10.1002/eqe.801

Porter, K. (2019). A Beginner's guide to fragility, vulnerability, and risk. University of Colorado Boulder, 126 pp., http://spot.colorado.edu/~porterka/Porter-beginnersguide.pdf.

Salvini S. (2017) Deterioration of carbonate rocks and vulnerability of cultural heritage in a changing climate, PhD Thesis.

Sundin, E., & Makkonen, L. (1998). Ice loads on a lattice tower estimated by weather station data. Journal of Applied Meteorology, 37(5), 523-529. DOI: 10.1175/1520-0450(1998)037<0523:ILOALT>2.0.CO;2

UNE 103-500-94. Geotecnia, Ensayo de Compactación, Proctor Normal. Norma Española. AENOR 1994.

Vamvatsikos, D. & Cornell, C. A. (2002). Incremental dynamic analysis. Earthquake Engineering & Structural Dynamics, 31(3), 491–514. DOI: 10.1002/eqe.141

Vivek, B., Sharma, S., Raychowdhury, P., & Ray-Chaudhri, S. (2017). A study on failure mechanism of self-supported electric poles through full-scale field testing.

Engineering Failure Analysis, 77, 102–117. DOI: 10.1016/j.engfailanal. 2016.12.019

Zeppos, J., Krommyda, M. & the HYPERION Consortium (2019). End User needs and practices report. Deliverable D2.1 URL https://www.hyperion-project.eu/deliverables/